AD 402 461

TRANSLATION

HEAT AND POWER ENGINEERING (SELECTED ARTICLES)

FOREIGN TECHNOLOGY DIVISION

AIR FORCE SYSTEMS COMMAND

WRIGHT-PATTERSON AIR FORCE BASE

OHIO

UNEDITED ROUGH DRAFT TRANSLATION

HEAT AND POWER ENGINEERING (Selected Articles)

English Pages: 61

SOURCE: Russian periodical, Teploenergetika, No. 3, 1961, pp. 100-107, 116-128, 137-163.

T2

SOV/665-61-0-3

PREPARED BY:

TRANSLATION SERVICES BRANCH
FOREIGN TECHNOLOGY DIVISION
WP-AFB, OHIO.

TABLE OF CONTENTS

THE DISTRIBUTION OF IMPURITIES IN THE ALLOYED LAYER OF PHOTOELECTRIC CONVERTERS

A. K. Zaytsev and A. Ya. Gliberman

Recently, much use has been made of various semiconductor devices prepared by the diffusion of donor or acceptor impurities and having large-surface p-n-junctions.

The properties of such a device, its characteristics, and its efficiency depend greatly on the alloyed surface layer and the distribution of the concentration of the active impurity in the layer. Therefore, it is very important to find an acceptable method for investigating the surface layer when developing diffuse semiconductor devices.

In the present work we give a method for investigating the layer created by the diffusion of acceptor impurities (boron) into n-type silicon, or a donor impurity (phosphorous) into p-type silicon. The device is intended to be used as a photoelectric radiant-energy converter.

Specimen Model and Measurement Method

The measurements were conducted using rectangular samples. The

resistivity was measured before diffusion of the impurity by the two-probe method according to a compensation system. On a special device we determined the Hall-effect voltage. The position of the sample during such a measurement is shown schematically in Fig. 1.*

On the basis of these measurements we calculated the basic parameters of the starting material: resistivity ρ, mobility μ, and concentration of main charge carriers n.

After diffusion, one side of the sample is completely polished; the alloyed layer is placed only in the centers of the side faces. As the contacts we used nickel which was then tinned. To the tinned contacts we attached wire current leads. The sample prepared for the experiments is show in Fig. 2.

The electrical properties of the sample as the alloyed layer was etched were investigated using the same devices as for determination of the starting material. After alloying, the current does not pass through the entire thickness of the sample but only through the thin surface layer, since the p-n-junction can be considered a plane which electrically insulates the starting material from the alloyed layer with a conductivity of the opposite type.

The entire sample, except for the upper working surface, was covered with lacquer. In this form the working surface was etched in a KOH solution. The lacquer was carefully removed from those parts of the sample which were to come in contact with the electrodes of the measurement devices. After measurement, the contacts were again coated with lacquer for subsequent etching.

---

* The projections on the side faces were created after the sample had been subjected to thermal diffusion.

Simultaneously with the etching, we measured the load characteristics of the sample operating as a photoelectric converter. The measurements were made under a lamp (3S3-type thermal radiator) corrected with light filters* with a spectrum and intensity of the solar radiator of 78 mw/cm^2.

We should mention that the position of the current lead on the alloyed working surface (Fig. 2) is extremely unsuitable, from the standpoint of creating minimum spreading resistance.

In addition, a lower efficiency results from the fact that the working surface of the sample has a high reflection factor because of the lack of a nonreflecting film on the working surface.

However, these facts do not disrupt the general regularity of the change in the electrical properties as the alloyed layer is etched.

The average thickness of the etched layer Δx was determined from the difference in weight before and after etching. Weighing was done on an analytical balance with a sensitivity of 10^{-4} per scale division. The specific weight of the silicon was 2.3 g/cm^3.

Strictly speaking, the removal of subsequent layers of the alloyed region by the etching method cannot pretend to any great accuracy because of the relatively rough nonuniform nature of the etching itself. Nevertheless, the averaged values obtained and the order of magnitude are completely reliable for appropriate conclusions to be drawn.

Calculation Formulas

In the alloyed region it is important to establish the dependence $\overline{C}_1 = f(x)$, where $\overline{C}_1$ is the average concentration of the embedded

* The lamp was adjusted using a standard photo-converter whose characteristic was determined in advance under illumination by natural sunlight of a known intensity.

impurity in each subsequently etched layer, and x is the depth of the layer calculated from the surface of the sample. The value of $\overline{C}_1$ should differ for each etched layer since the impurity is non uniformly distributed in the alloyed region. In our specific case, considering that the atoms of the impurity are all ionized [1], we can assume that $\overline{C}_1$ is equal to the average concentration of the basic current carriers in the etched layers.

Two independent measurements were made each time to determine this concentration for the alloyed layer.

Measurement of the Layer Conductivity Layer G from the Remaining Alloyed Layer

The ends of the sample were clamped between two electrodes and current I (of the order of 10-20 ma) was passed through it. The drop in voltage U was determined between two tungsten probes located along the current lines and 1 mm from them.

Then

$$G = \frac{I \cdot l_0}{Ub} \left[\frac{1}{\text{ohm}}\right], \qquad (1)$$

where l_0 is the distance between probes, in cm; and b is the width of the sample, in cm.

Measurement of the Emf of the Hall Effect

The sample was placed in magnetic field H such that the magnetic lines of force were perpendicular to the working surface. Along the zones alloyed with the impurity we passed current i and determined the voltage drop U_e between the ends of the sample. The Hall-effect voltage U_H was read between the projections of the sample in the middle of its side faces (Fig. 1).

Knowing U_H and G before and after etching we can, using formulas derived previously [1, 2], find the value of the average mobility $\bar{\mu}_1$ and the average concentration of atoms of the impurity (boron) $\bar{C}_1$ in the thin etched alloyed surface layers of silicon:

$$\bar{\mu}_1 = \frac{\frac{U_{H0}}{B} - \frac{U_{H1}}{B} \cdot \frac{G_1}{G_0}}{1 - \frac{G_1}{G_0}}; \quad (2)$$

$$\bar{C}_1 = \frac{G_0 - G_1}{q\bar{\mu}_1 \Delta x}, \quad (3)$$

where the subscript "0" pertains to values found before removal, and the subscript "1" pertains to values found after removal, of a thin layer Δx thick, in cm; B is a constant, equal to $1.18 \cdot 10^{-3}$ HbE_e (in our case, $E_e = U_e/l$, where l is the length of the sample, cm); q is the electron charge of $1.6 \cdot 10^{-19}$ coulomb; U_e and U_H are in volts; and H is in gauss.

For a more accurate calculation of $\bar{\mu}_1$ it is better to proceed as follows. First we construct, from experimental points, and dependences $U = f(x)$ and $U_H = f(x)$ (Fig. 3). Then using strictly determined thicknesses Δx (e.g., $\Delta x = 1$ or $\Delta x = 2\mu$) and finding from the graphs the values of U and U_H corresponding to the selected Δx, we can calculate for them $\bar{\mu}_1$ and $\bar{C}_1$ for the entire alloyed region.

Results

When the diffusion of atoms occurs from the vapor phase (on diffusion of phosphorous) or from a relatively thick layer of atoms of the diffusing agent which has been precipitated onto the surface of the silicon (on the diffusion of boron), we can consider that the number of source atoms remains constant during diffusion. In this case, as we know [3], the concentration of the diffused atoms is determined by the expression

$$C_{xt} = C_0 \operatorname{erfc} \frac{x}{\sqrt{4Dt}} \quad [cm^{-3}], \qquad (4)$$

where C_{xt} is the concentration of imbedded impurity diffused in t seconds over a distance of x cm; C_0 is the concentration of impurity atoms at the surface, cm^{-3}; D is the diffusion coefficient, cm^2/sec; and erfc is a table function.

Investigations conducted on several samples for which the p-n junction was created by the diffusion of phosphorous in p-type Si [2] (Fig. 4) showed that the distribution of impurity atoms in the alloyed region is unique. The same was true of boron in the creation of a p-n junction with n-type Si. The concentration of phosphorous and boron, when shifting from the surface to the p-n junction, changed relatively little (by approximately one order of magnitude) throughout practically the entire alloyed layer, and dropped sharply (by several orders of magnitude) near the p-n junction.

This can be explained by the fact that the diffusion coefficient of the impurity is not the same throughout the alloyed layer.

An approximate evaluation, made on the basis of experimental data [2], showed that near the surface the diffusion coefficient was 10-14 times greater than with the sample, at the p-n junction. In other words, we have a "steep diffusion front" of impurity in the silicon.

The curves shown in Fig. 4 pertain to three samples whose starting material had identical resistivity. The point of intersection of the diffusion curve with the horizontal straight line corresponding to the impurity concentration in the starting material gives the depth of occurrence of the p-n junction. The reason for the discrepancy between the theoretical distribution of the diffused impurity and experimental data has not yet been explained, and requires further study.

Evidently, specific conditions of the process of the diffusion of

an impurity into silicon, which cannot be taken into account in the general diffusion theory, play a role here.

Figure 5 shows changes in the electrical properties of a sample as a photoconverter.

We see that upon first etching the alloyed zone, there is an increase in the open-circuit voltage U_{o-c}, the short-circuit current I_{s-c}, and the maximum power P_{max} of the photoconverter.

This increase occurs to a specific depth of the p-n junction, which can be called the optimum depth. Further etching results in a decrease in the indicated parameters.

When the p-n junction is deeper than x_{opt}, the resistance $\underline{r}$ of the layer increases slowly. For junction depths less than x_{opt} the resistance of the alloyed layer sharply increases. In our specific case (Fig. 4) x_{opt} is equal to approximately 3 μ [4].

Analysis of the distribution of the concentration of the imbedded impurity and the change in the parameters of the sample as a photoconverter as the alloyed region is etched, conducted for many samples, makes it possible to make the following assumptions.

The optimum depth of the p-n junction, corresponding to the maximum power generated by the photoconverter, can be defined mainly by two values: the total value of surface and volume recombination of the s-type carriers, and the successive resistance R_s of the photoconverter. To lower the recombination losses it is necessary that the p-n junction be removed from the region where the pairs form by a distance equal to or less than the diffusion length of the current carriers.

Electron-hole pairs occurring under the influence of light form approximately to a depth of 25 μ from the surface [5]. Therefore,

for deep junctions we can consider that all pairs are generated in the alloyed region. In this case the coefficient of the separation of pairs by the p-n junction will depend mainly on the diffusion length of the secondary current carriers of the alloyed zone.

As the surface is etched, the alloyed zone becomes thinner and when the sample is illuminated, the relative number of pairs formed on the part of the starting silicon increases.

Now the separation coefficient will depend on the diffusion length of the minority carriers of the alloyed region and on the diffusion length of the minority carriers in the starting material.

The optimum depth of the p-n junction x_{opt} will evidently depend on the relation between these diffusion lengths and the concentration of electron-hole pairs on both sides of the p-n junction.

The successive resistance of the photoconverter consists of the sum of several resistances:

$$R_s = R_1 + R_{Si} + R_c$$

where R_1 is the resistance of the upper layer alloyed with impurities; R_{Si} is the resistance of the starting silicon; and R_c is the resistance of the contacts of the photoconverters.

With etching of the surface ($R_{Si} + R_c$) the back resistance remains constant, while R_1 increases due to a decrease in the thickness of the alloyed region.

This can also effect the terminal value of x_{opt}, shifting it toward higher values compared with that value which would result only from the influence of recombination.

The influence of R_1 on the shift in x_{opt} can possibly explain the experimental fact (see Fig. 5) that the depth of the junction, which corresponds to maximum efficiency of the photoelement, is greater

than the depth of the junction corresponding to maximum I_{s-c}.

We can also assume that the terminal value of x_{opt} is also effected by the back resistance of the photoconverter, since it has been shown [6] that beginning with specific photoelement dimensions, its back resistance sharply increases. Photoconverters for which the p-n junction was created under identical conditions should, with different parameters, have differing x_{opt}.

The final value of the optimum depth of the p-n junction corresponds to that value for which the total effect of all the enumerated factors is minimum.

Conclusions

1. The described method is applicable to study of impurities in the surface layer of photoconverters.

2. For photoconverters with an upper alloyed layer formed by the diffusion of boron into n-type silicon and phosphorous into p-type silicon, the distribution of the imbedded impurity is not subject to Fick's law. The diffusion front is steep, i.e., the impurity concentration changes relatively little throughout the alloyed layer, and drops sharply at a slight distance from the p-n junction.

3. The optimum depth of the p-n junction is evidently determined by the following factors: recombination, the resistance of the alloyed layer, and the value of the back resistance R_b. The optimum depth occurs where all these factors are minimum.

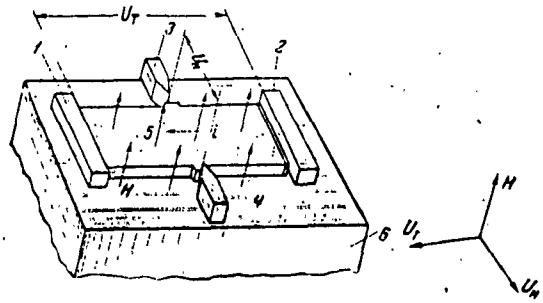

Fig. 1. Device for measuring the Hall-effect voltage. 1-2) current-conducting electrodes; 3-4) electrodes for measuring the Hall-effect voltage; 5) sample; 6) bottom pole of the electromagnet.

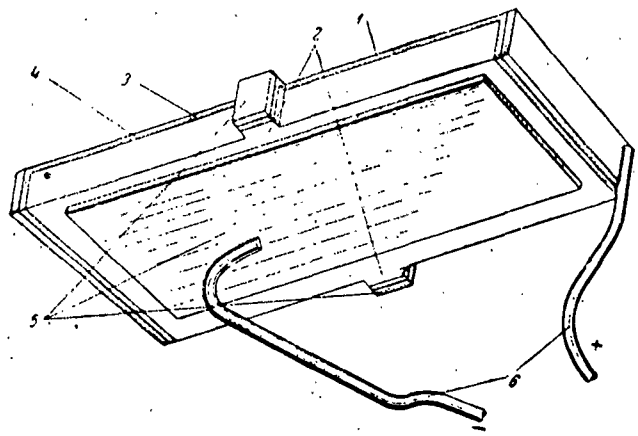

Fig. 2. Sample for investigating the alloyed layer. 1) p-n junction, 2) electrode projections for measuring the Hall-effect, 3) diffused layer, 4) starting silicon, 5) metal contacts, 6) current leads.

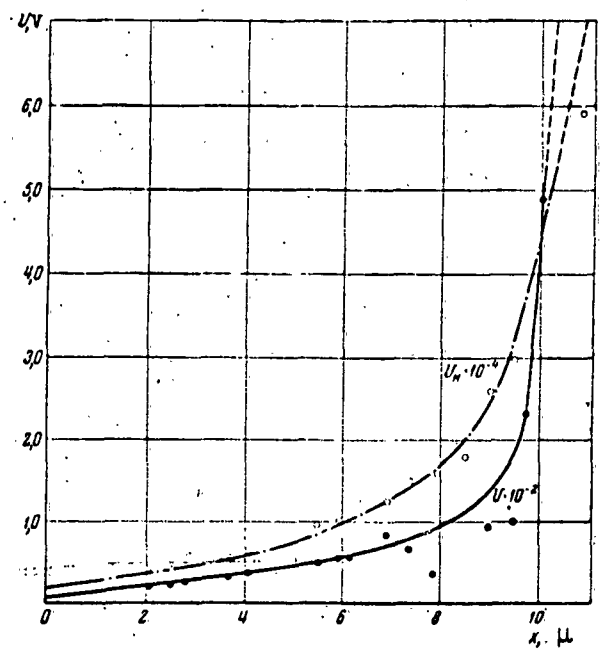

Fig. 3. Voltage V_H and V vs. depth of layer x.

Fig. 4. Distribution of concentration of phosphorous atoms diffused into a p-type silicon surface layer.

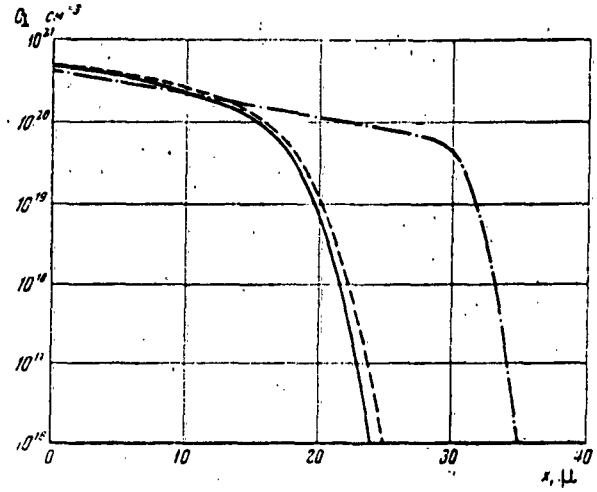

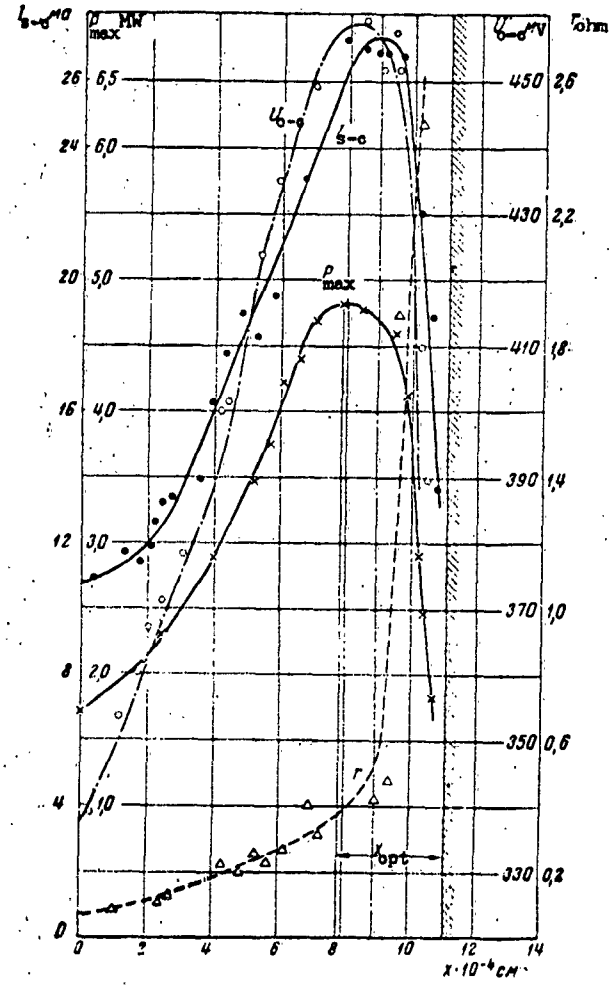

Fig. 5. Electrical properties of sample vs. depth of the p-n junction.

REFERENCES

1. V. K. Subashev and S. A. Poltinnikov. Opredeleniye podvizhnosti i kontsentratsii nositeley toka v poverkhnostnom sloye poluprovodnika. Fizika tverdogo tela, Vol. 2, No. 6, 1960, 1169-1177.

2. V. K. Subashev et al. Raspredeleniye atomov forfora pri diffuzii v kremniy (in press).

3. G. Backenstoss. Evaluation of the surface concentration of diffused. Bell system tech., No. 37, 1958, 69-710.

4. D. M. Chapin, C. S. Fuller, G. L. Pearson. The bell solar battery. Bell Laboratories Record, No. 7, 1955, 242-246.

5. V. S. Vavilov. Solnechnyye batarei. Atomnaya energiya, Vol. 1, No. 3, 1956.

6. A. Ya. Gliberman and R. P. Fedoseyeva. Issledovaniye faktorov, vliyayushchikh na posledovatel'noye soprotivleniye i drugiye parametry fotopreobrazovateley iz kremniya, Teploenergetika, No. 3, 1961, 91-99.

A STUDY OF THE POSSIBILITY OF USING POLYCRYSTALLINE SILICON TO MAKE PHOTOELECTRIC CONVERTERS

A. Ya. Gliberman, A. K. Zaytseva, and A. P. Landsman

Up to the present time, highly efficient silicon photoconverters have been made only of single crystals, which are still extremely costly. The use of less expensive polycrystals involves great difficulties in the attaining of suitable efficiency.

Preliminary investigations using single-crystal silicon have made it possible to determine the effect that a number of parameters of the starting material have on the properties of the photoconverters. These works have, to a considerable extent, made it possible to show the possibility of using polycrystals in the manufacture of photoconverters; basically, this is as follows.

It is considered that it is most favorable, from an energy standpoint, to make the converters along the crystallographic direction (111).* However, studies of single crystals [1] have shown that the energy properties of photoelements do not depend on the crystallographic orientation of the silicon used to make them. The crystallographic

* Such an opinion is evidently based on concepts of the properties of fused p-n junctions.

planes (111), (110), and (100) have no advantage over one another. The rate of diffusion of boron and phosphorous in silicon is identical along all crystallographic directions. The efficiencies of converters made of plates cut along the above-indicated planes were completely identical. Further, it was noted that the quality of silicon photoconverters is independent, within broad limits, of the resistivity ρ of the starting material and the life time τ of the minority carriers (we investigated the intervals ρ = 0.1-4.0 ohm and τ = 1-100 μsec) [2].* The above results allowed us to propose the use, as a raw material for making solar converters, of such polycrystalline silicon in which, from grain to grain, there can be considerably greater variations of ρ and τ than along a single-crystal fusion, while the crystallographic orientations of individual single-crystal grains can differ sharply.

Polycrystalline Silicon

A polycrystal consists of single-crystal grains with varying orientation of the crystallographic axes. The basic part of the impurities may accumulate at the boundaries of the crystal grains. In semiconductors with low conductivity the presence of such transitional layers with increased concentration can, in certain cases, have the result that when an electric current is passed through, a considerable part of it will flow not through the single-crystal grains but along the surface of the grains which has increased impurity conductivity. On the other hand, in polycrystalline silicon the boundaries of the grains can act as regions with increases resistance and, when measuring the sample resistance, they can appear as potential jumps. The

* In this work we do not study the influence of life-time restoration on the properties of photoconverters.

presence of adsorbing impurities on the grain surface can influence, to a considerable extent, the photoconductivity of the polycrystals since the current carriers freed by the light can be captured by intercrystalline layers, which results in sharply limited mobility of the current carriers.

There may be cases when despite the absence of adsorbing impurities the atoms on the grain boundaries are in a somewhat different energy state than are the atoms of the basic substance which are located far from the boundaries. This latter fact results in the formation of basic "surface levels" (Tamm levels) which can be located in the forbidden zone and cause surface conductivity. The presence of surface levels can influence noticeably not only the dark conductivity of the polycrystals but also the photoelectric, contact, and other properties. It follows from experimental data that the mobility, and particularly the lifetime of the current carriers of the polycrystals are, as a rule, less than for single crystals, which is due in particular to the fact that the grain boundaries act as regions with a high recombination rate [3].

Consequently, the field of application of polycrystal semiconductors is still quite limited. The literature contains no data on photoconductors made of polycrystalline silicon, except for the publication [4] which mentions the manufacture of elements made of large-block crystals. However, their efficiency did not exceed 0.6%, which eliminated them as an electric power source.

The investigated polycrystalline silicon can be characterized by the sign of the conductance (p- or n-type), the degree of polycrystallinity (the magnitude of the individual single-crystal grains), and also by the method of preparing the ingot, i.e., whether an oriented

or nonoriented seed is used to produce the crystal. In the first case, individual single-crystal "needles" of relative large cross section (Fig. 1a) penetrated longitudinally throughout practically the entire ingot (henceforth we will call this an oriented crystal). We can assume that the crystallographic orientation of the perpendicular axis of the ingot of the cross-section plane of individual single-crystal grains varies, from needle to needle, within certain limits about the crystallographic plane (111). In the second case, when the crystal is produced without the aid of oriented seeding, the individual single-crystal grains are positioned at random, so that in the cross section perpendicular to the axis of the fusion there will be the most diverse orientations of the individual crystals.

The dimensions of the grains in the second case (nonoriented crystal, Fig. 1b) were considerably smaller than in the case of the oriented seed. When X-rays were taken of several large-block crystals elongated by means of the seed oriented in the (111) plane, it was found that the planes of the individual single-crystal grains in the cross section perpendicular to the crystal axis were randomly oriented and did not lie within a small angular range near the (111) plane. Table 1 gives the angles, averaged for many grains, between the crystallographic planes (110), (100), (111), and the plane of the cut, i.e., the plane perpendicular to the crystal axis, for several polycrystalline oriented ingots.

We see that the deviation of the plane of the cut from the (110) and (111) planes is approximately identical. We can say that regardless of whether the polycrystalline ingot is elongated by means of an oriented or nonoriented seed, there is no predominant orientation of the individual single-crystal grains above any crystallographic direction.

Investigation of the resistivity of polycrystals showed that it, as a rule, remains constant from grain to grain, while the boundaries between the grains can be regions with increased resistance. Similar jumps in resistance were detected for more high-resistance materials ($\rho \sim 1$ ohm·cm and higher) and were completely absent in low-resistance materials ($\rho \sim 0.1$ ohm·cm). Figure 2 gives graphs of the voltage drop along rectangular polycrystalline samples. The voltage was measured by a potentiometer between two probes along the longitudinal axis of symmetry of the sample. One probe, the fixed one, was located near one of the contacts, and the other was moved along the sample. The boundaries between the grains are indicated by the wavy lines. The identical slope of the voltage line for various grains indicates that their resistivities are identical. The rapid changes in voltage at the boundaries are cuased by the sharp increase, in this region, of the resistance. The nature of the intercrystal resistances has not as yet been sufficiently studied. Preliminary measurements, however, have shown that the resistances do not evidently pertain either to the type of purely capacitive layers or the type of barrier layers in the form of a p-n junction, since the change indirection of the direct current and the transition to alternating current with frequency variations from 50 to 200 cps did not lead to a change in the value of the transitional resistance between the individual grains (Fig. 3). A change in the value of the current passing through the sample also resulted in no change in the value of the intercrystal resistances. This indicates that evidently the nature of this resistance cannot be classified as symmetrically-nonlinear. In the case of illumination, the resistance of the sample decreases, mainly due to the photoconductivity occurring in the intercrystal regions. With a rise in temperature,

in the darkness, the resistance of the intercrystal regions also decreases while the resistivity of the single-crystal grains increases somewhat. This fact does not contradict the experimental dependences of the value of the resistivity on temperature for silicon with varying amounts of proportioned impurities of atoms [3]. This makes it possible to assume that the transient resistances between the grains are ohmic, while the observed rapid changes are due to the lower effective impurity concentration in these transitional layers.

The Hall voltage also changes considerably along the sample. In several cases this is a two-fold change. The scatter cannot be caused by edge effects since a similar variation in the Hall voltage was also noted in the central part of the polycrystalline samples. In single-crystal plates the scatter of the values of the Hall voltage, measured at the center and near the current contacts, was considerably less.

As we have mentioned, the rate of diffusion of boron and phosphorous into sodium is identical (within limits of measurement accuracy $\sim 1\ \mu$) in all crystallographic directions. An example of the position of the p-n junction for polycrystals is given in Fig. 4, which shows microsections with a tinted p-n junction.

As can be seen from the photographs, the depth of the p-n junction is identical in all grains of a polycrystalline plate. There was no noted disruption of the diffusion layer in the intercrystalline regions, as a rule, although there were samples where the diffusing agent penetrated to a great depth at the grain boundaries (Fig. 5). The nature of these disruptions was evidently caused, for the cases shown in Figs. 5a and 5b, by various factors, i.e., by the varying structure of the boundary region. Figures 5a and 5b show two intensely colored bands along the edges of an intermediate zone. The example

(phosphorous) was evidently concentrated on both sides of this zone. In another sample (Fig. 5b) the impurity penetrated deeply along the joint, and there is no weakly colored intermediate zone. The nature of these disruptions is not yet clear. Such disruptions should undoubtedly have a negative influence on the properties of photoconverters.

Concepts on the Design of Polycrystal Devices

It could be assumed that in the present design of instruments the influence of certain harmful phenomena, which might occur at the boundaries of relatively large grains (Fig. 1a, b), could be excluded to a considerable extent, since the generated pairs, before their separation (Fig. 6) in most cases could not pass the boundary zone. The influence of intercrystalline layers will be reflected only in the pairs formed in the immediate vicinity of the boundary zone. The number of pairs will evidently be the greater, the higher the degree of polycrystallinity of the workpieces. Obviously, we can consider that if the dimensions of the crystal grains are much greater than the diffusion length of the minority current carriers (even better, greater than the thickness of the instrument plate), the amount of carriers recombined at the grain boundaries, not counting the pairs generated in their immediate vicinity, will be very slight. The harmful influence of the increased resistance of the intercrystal junctions can be eliminated by means of a special current conducting network (Fig. 7). In this case, the converter consists, as it were, of individual small single-crystal photoelements connected in parallel [5]. However, at the present time the difference in resistance can be balanced by means of thermal diffusion or by coating with a good-conducting surface film, which makes it possible to eliminate the placing

of an additional current network on the illuminated surface of the polycrystalline device.

The accumulation of impurities in the intercrystalline region is most harmful to the converter. Increased concentration of these impurities can result in shunting of the p-n junction. Such phenomena were observed when making instruments from low-resistance polycrystalline ingots.

Operational Characteristics of Polycrystalline Converters

Photoconverters were made from oriented and nonoriented p- and n-type polycrystalline ingots.

In general, we may say that the operational characteristics of polycrystalline converters and the influence on them of various external factors (illumination, temperature, etc.) differ little from photocells made from single crystals. The basic distinction of polycrystalline devices is the somewhat lower open-circuit voltage V_{o-c} and short-circuit current density I_{s-c} which, naturally, causes lower efficiency.

Figure 8a shows the load characteristics of four polycrystalline converters, recorded in sunlight in the middle of July, 1959, in Moscow. The converters were made of oriented p-type polycrystals with grain structures as shown in Fig. 1a. Figure 8b shows analogous characteristics for devices made of nonoriented p-type polycrystals (see Fig. 1b). The curves were recorded on October 31, 1959 at Moscow. In general cases the p-n junction was made by thermal diffusion of phosphorous vapors into silicon. For n-type polycrystalline converters (grain structure shown in Fig. 1a) the p-n junction was made by diffusion of boron from the solid phase into silicon.

Table 2 gives the basic parameters of a number of elements from

all the mentioned groups. The light parameters given in the table (V_{o-c}, I_{s-c}, efficiency) were obtained by means of a heat radiator (a ZS3 bulb) using a water filter with a photoconverter temperature of ~50°. The lamp was adjusted such that the load curve of the standard element, recorded under the lamp, coincided with the load curve of the same element under sunlight with a total intensity of about 750 w/m^2. The values of the series R_s and parallel R_p resistances of the photoconverters were determined, respectively, from the direct and reverse branches of the dark volt-ampere characteristics. The values of the density of the dark saturation current j_0 and the coefficient A* were calculated from the logarithmic equation of the direct branches of the volt-ampere characteristics recorded at a temperature of ~25°.

Polycrystalline cells can be divided into two types according to the values of j_0 and the parameter A. For some of these (Fig. 9), because of the break in the logarithmic line $\ln I = f(V)$, the values of A and j_0 were different for low and high voltages (the table gives both values). The break is usually noted in the range of voltages from 250 to 450 mv. For other cells, the coefficient A and the value of j_0 remain constant from low positive voltages up to voltages at the p-n junction close to the value of the potential barrier of the junction V_k. A similar phenomenon was observed for single-crystal photoconverters [6]. The reason for this is not clear.

The temperature dependences of the basic parameters of polycrystalline converters – open-circuit voltage, short-circuit current, series resistance, and maximum power – are the same as for single-crystal

---

* A is a coefficient which characterizes, to a certain extent, the width of the p-n junction; it is within the range from one to several units.

converters [6, 7, 8, 9]. However, sometimes at low temperatures there are very high series resistances. With a drop in the temperature of several samples from +25 to -60° the resistance measured from the slope of the linear segment of the volt-ampere characteristic increased 100-fold. The value of the maximum power underwent a 2-3-fold decrease from its maximum value. The same type of sharp increase in series resistance with a drop in temperature was observed for photocells made from polycrystals with resistance discontinuities at the boundary layers. That such a great increase in series resistance does not cause a considerable decrease in power can be explained by the fact that the light volt-ampere characteristic of these converters has two linear segments. In the fourth quadrant, where the device operates as a generator, the slope of the linear segment of the volt-ampere characteristic (Fig. 10) and, consequently, the series resistance in this quadrant, are considerably less than in the first quadrant. The slope of the linear segment in the first quadrant sharply increases with a drop in temperature, and the slope of the linear segment in the fourth quadrant remains practically constant. The nature of the non-linear resistance in the region of voltages of 500-800 mv is unclear. It is possible that such an inflection is caused by the influence of the blocking layer of the lower contact which is manifested at a low temperature. This layer in the first quadrant is included in the blocking direction.

The maximum spectral sensitivity of the polycrystalline photo-converters (Fig. 11) is in the wavelength region 7500-8500 A. Illumination of the polycrystalline devices lowers the reflection coefficient from 30 to 5-8%. The maximum power produced per unit working surface of an average polycrystalline converter reaches, in sunlight, 5-6 mw/cm^2 at present. Batteries with a power of 1 w made from

polycrystalline silicon are 2-3 times less expensive than those made of single-crystal silicon. Therefore, despite the somewhat lower energy indices of the photocells, polycrystalline silicon can be a promising material for mass-production of photoelectric converters.

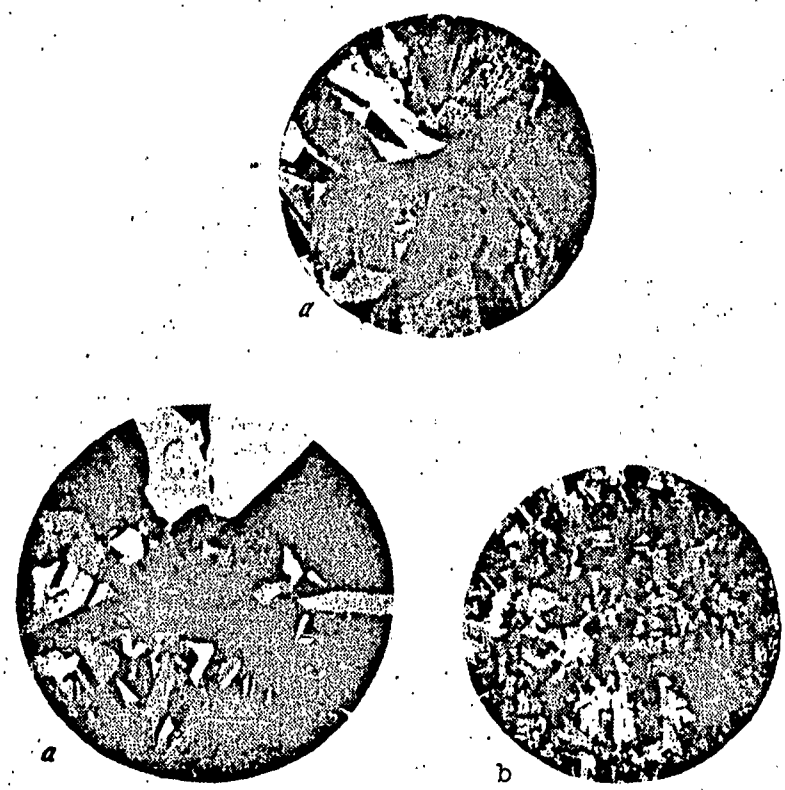

Fig. 1. Samples of polycrystals.
a) oriented, b) nonoriented.

TABLE 1

Ingot	Deviation from crystallographic directions, deg.			Number of grains for which averaging was done
	(100)	(110)	(111)	
1	38,8	21;2	21,3	8
2	38,8	21,2	22,0	17
3	38,5	25,3	20,0	6

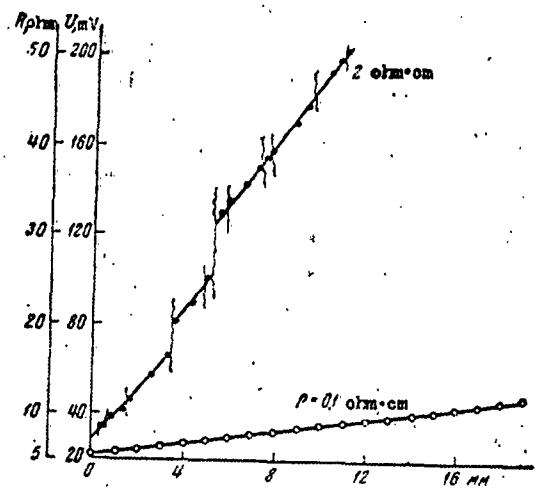

Fig. 2. Graphs of the voltage drop along rectangular polycrystalline samples.

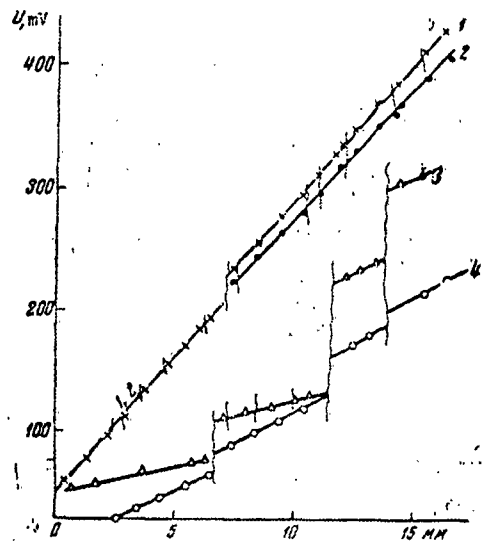

Fig. 3. Change in the voltage drop of a polycrystalline sample under the influence of temperature and illumination. 1) darkened sample No. 1 at 25°; 2) sample No. 1 under 2000-lux illumination and at 25°; 3) sample No. 2 at 25°; 4) darkened sample No. 2 at t ~ +150°.

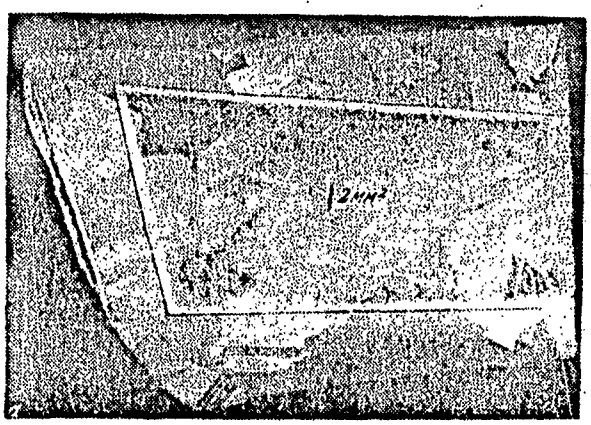

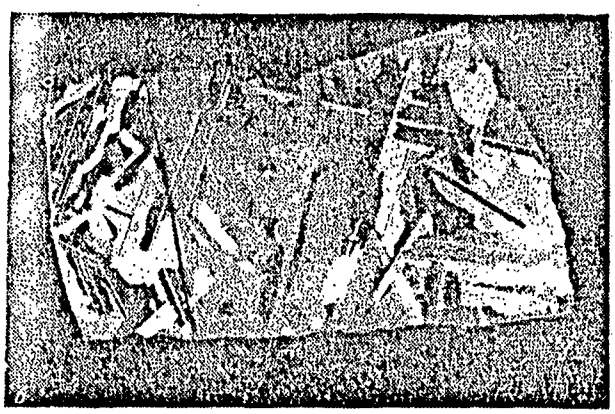

Fig. 4. Photographs of microsections with a p-n junction in polycrystals. a) oriented large-block crystal, ρ ~ 2.0 ohm·cm, depth of junction 15 μ; b) nonoriented small-block crystal, ρ ~ 0.1 ohm·cm, depth of junction 6 μ

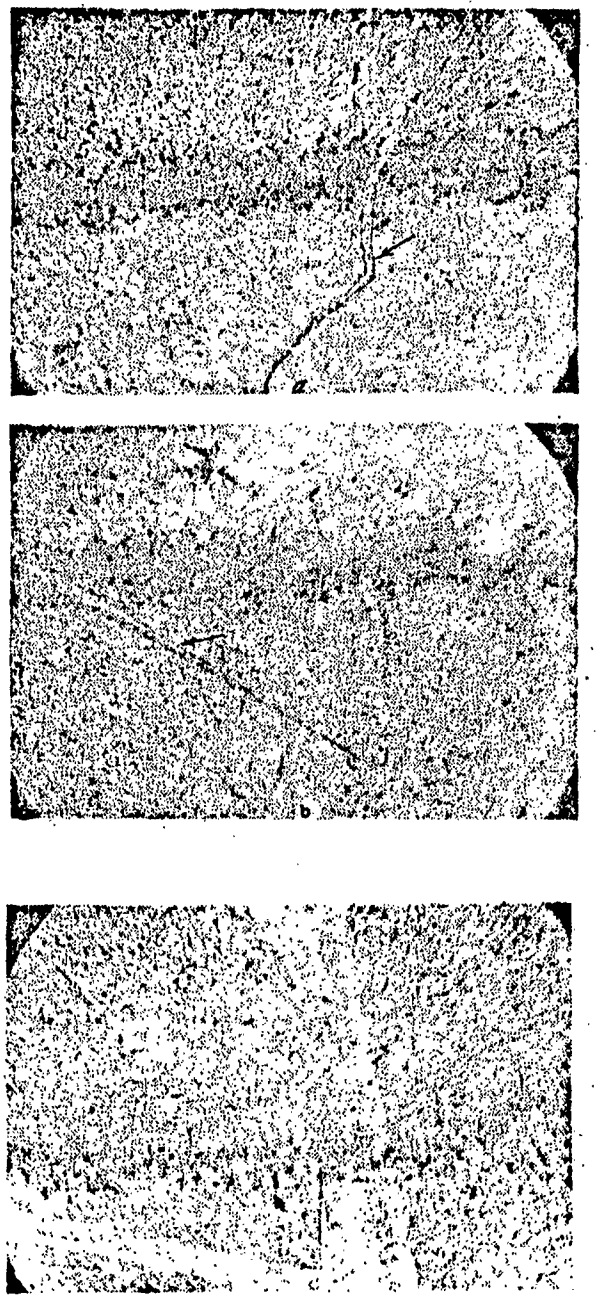

Fig. 5. Views of the disruption of the diffusion layer in intercrystalline regions (52.5x) a,b) disruptions with an intermediate zone; c) without an intermediate zone.

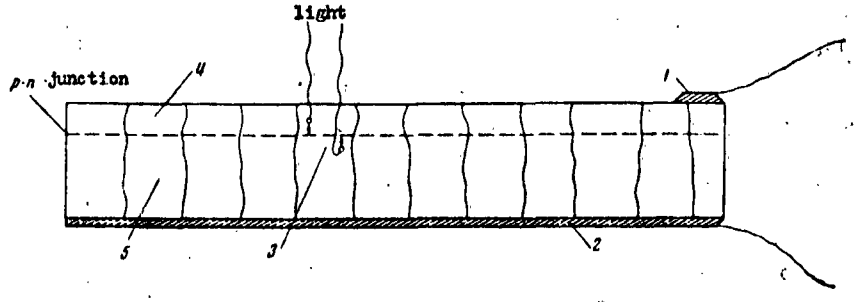

Fig. 6. Schematic position of grains in a polycrystalline photoconductor (cross section). 1,2) upper and lower contacts; 3) diffusion of minority carriers to p-n junction; 4) n-type; 5) p-type.

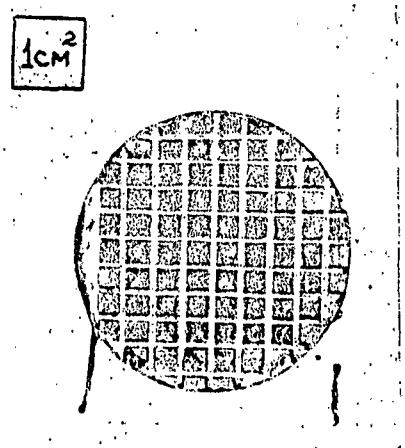

Fig. 7. Polycrystalline converter with additional current conducting networks.

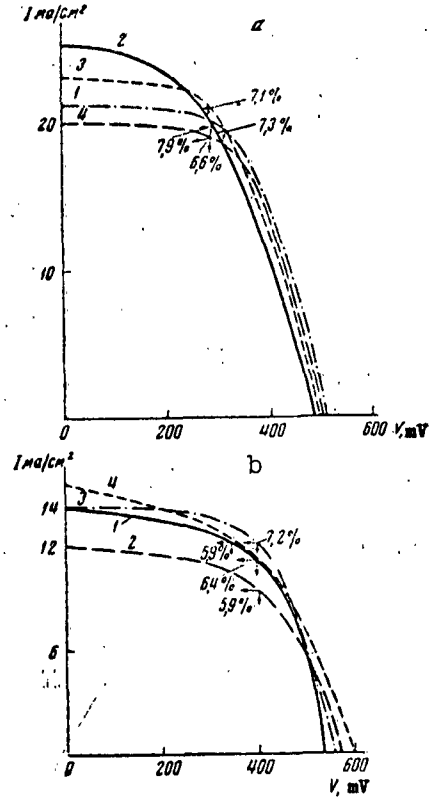

Fig. 8. Volt-ampere load characteristics of converters. a) converter made from p-type oriented silicon; 1) area of polycrystal 3.2 cm^2, intensity of sun's rays W = 915 w/m^2; 2) area 7, intensity 885; 3) 5.7 and 888; 4) 4.6 and 896; b) converter made of p-type nonoriented silicon; 1) area of polycrystal 3.6 cm^2, intensity of sun's rays 734 w/m^2; 2) 4.93 and 737; 3) 3.6 and 737; 4) 3.34 and 739.

TABLE 2

Sample Index	S, cm^2	V_{o-c}, mV	I_{s-c}, $\frac{ma}{cm^2}$	eff. %	R_S, ohm	R_p, ohm	A	I_o, $10^{-6}\frac{a}{cm^2}$
			Oriented p-type crystal				p = 2 ohm·cm	
1-O	7,0	510	22	6,4	1,3	2 000	2,5	0,3
								0,04
11-O	3,2	505	22	7,4	1,8	2 500	2,1	1,3
							1,3	0,04
20-O	4,6	490	21	6,4	1,4	4 000	2,4	1,5
							1,7	0,5
32-O	6,6	460	22	5,0	2,4	1 300	3,7	82
							1,3	6,7
			Nonoriented p-type crystal				p ~ 0,1 ohm·cm	
3-H	3,6	525	13	5,0	2,0	1 200	2,5	1,0
							1,6	0,02
4-H	3,6	490	16	4,8	1,5	10 000	2,9	1,2
							1,9	0,1
5-H	4,9	510	12	4,3	1,5	6 000	2,5	0,9
							1,5	0,04
8-H	4,1	510	14	4,2	1,5	1 600	3,0	1,0
							2,4	0,04
			Oriented n-type crystal				ρ ~ 1,5 ohm·cm	
O-20	11,0	495	18	5,0	0,6	300	4;6	105
O-32	10,9	490	14	4,0	0,6	1 600	3,4	23,0
O-27	9,4	500	17	5,0	0,4	1 900	1,1	7,4

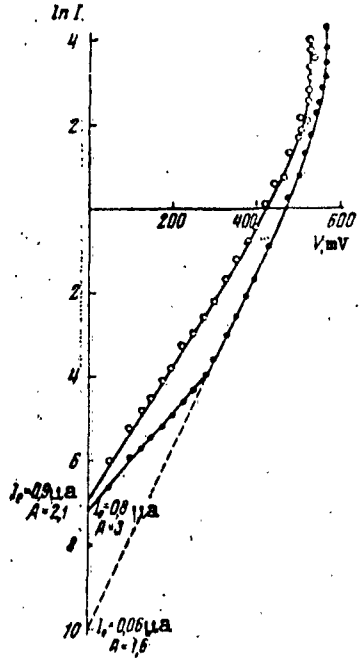

Fig. 9. Graphs of the equation ln I = f(V) for polycrystalline converters.

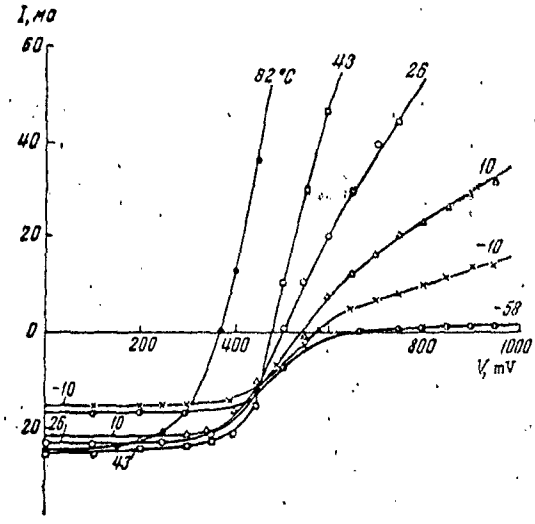

Fig. 10. Light volt-ampere characteristics of a polycrystalline converter at various temperatures.

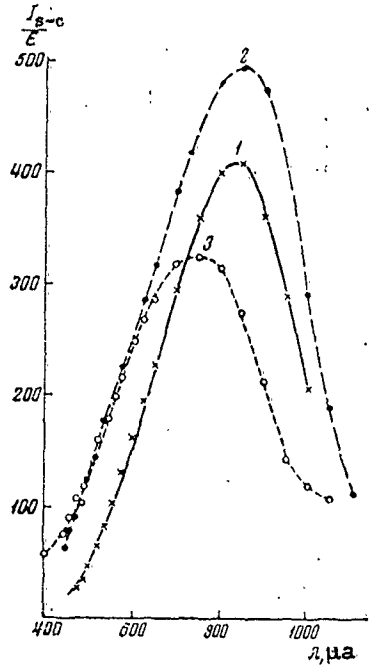

Fig. 11. Graphs of the absolute spectral sensitivity of polycrystalline photoconverters. 1) oriented p-type; 2) non-oriented p-type; 3) oriented n-type.

REFERENCES

1. A. Ya. Gliberman and O. P. Fedoseyeva. Issledovaniye vliyaniya kristallograficheskoy orientatsii kremniya na svoystva fotopreobrazovateley. Fizika tverdogo tela, No. 10, 1960.

2. A. Ya. Gliberman, et al. Vliyaniye udel'nogo soprotivleniya i vremeni zhizni neosnovnykh nositeley iskhodnogo materiala na kachestvo kremniyevykh preobrazovateley solnechnoy energii (in press).

3. S. S. Shalyt. Elektroprovodnost' poluprovodnikov. In the collection: Poluprovodniki v nauke i tekhnike, Vol. I, Izd. Akad. Nauk SSSR, 1957.

4. Yu. P. Maslakovets, et al. Fotelektricheskiye preobrazovateli solnechnoy energii iz p-kremniya. Zhur. tekh. fiz., 1956, Vol. 10, No. 10.

5. A. Ya. Gliberman et al. Fotoelektricheskiye preobrazovateli iz polikristallicheskogo kremniya. Fizika tverdogo tela, No. 8, 1960.

6. M. Prince. Silicon Solar Energy Converters. J Appl. Phys., 26 (5), 1955, 534.

7. V. S. Vavilov et al. Issledovaniye kremniyevykh fotoelementov kak preobrazovateley solnechnogo izlucheniya. Atomnaya energiya, Vol. 4, No. 6, 1958.

8. V. K. Subashiyev and M. Sominskiy. Poluprovodnikovyye fotoelementy. In the collection: Poluprovodniki v nauke i tekhnike., Vol. II, Izd. Akad. Nauk SSSR, 1958.

9. A. Ya. Gliberman and O. P. Fedoseyeva. Temperaturnaya zavisimost' nekotorykh parametrov kremniyevykh fotopreobrazovateley (in press).

DESIGNS AND ELECTRICAL CHARACTERISTICS OF BATTERIES MADE FROM SILICON PHOTOELECTRIC CONVERTERS

G. S. Daletskiy and N. V. Shavrin

At the present time there is a great difference in the design of batteries made from silicon photoconverters. The samples of batteries and photoconverters shown at the All-Union House of the National Economy differ in size, shape, geometry of the current conductors, and armoring. The diversity is due to the following reasons:

the high cost of single-crystal silicon used in the batteries;

the desire to use most effeciently the area allotted to the batteries;

the differences in the mechanical and climatic requirements imposed on the batteries.

The high cost of silicon requires that it be used as economically as possible and, consequently, the use of round photoconverters of various diameters, since silicon is prepared in the form of cylindrical ingots. Efficient use of the area requires the making of rectangular photoconverters, which results in great waste of the silicon. Either form can be used, depending on the intended purpose of the batteries.

Recently, due to the decreased cost of silicon, the creation of batteries from polycrystalline silicon, and mainly because of the ever increasing orders for batteries, there has been a tendency to standardize ready-made photoconverters, i.e., the production of 3-4 sizes of silicon photoconverters. These are made in the form of separate units (Fig. 1).

When there are no limitations on the sizes of the batteries, we use round photoconverters with radial and annular upper current conductors.

To increase the mechanical strength, the round photoconverters are placed in metal or plastic holders and insulating material is poured in. The surface is coated with special lacquers to protect against wear.

The diameter of the round photoconverter varies from 22 to 45 mm and depends on the diameter of the single crystal from which the photoconverter is made.

Regardless of the diameter, round photoconverters have identical electrical characteristics for solar radiation with an intensity of 100 mw/cm^2 and a temperature on the cell of 30°.

At maximum power the efficiency is 7-9%; the maximum specific power is 7-0 mw/cm^2; the voltage at maximum power is 0.38-0.40 v; the current, at maximum power, from 1 cm^2 of working surface is 20-24 ma.

Rectangular photoconverters are used to make many types of batteries with power from fractions of a watt to hundreds of watts.

In order to facilitate the mechanization and automation of photocell production and to simplify and assembly and mounting of batteries, the number of sizes of manufactured photoconverters has been reduced greatly.

The table gives the basic electrical characteristics of certain standardized photoconverters with an output voltage of 0.4 v with solar radiation energy of 100 mw/cm^2 and a cell temperature of 30°.

Combined use of the four sizes of photoconverters shown in Table 1 makes it possible to increase the surface utilization factor of almost any battery to 0.9 (to 0.95 in the case of rectangular forms).

Silicon photoconverters of various types are grouped as cells and groups (Fig. 2).

Each cell consists of 8 series-connected photoconverters. The converters overlap, which assures reliable electrical contact and maximum utilization of the surface of the battery.

Current conductors are affixed to the terminal photoconverters to connect the cells into groups and batteries.

The choice of the number of photoconverters in a cell is not fortuitous. Each cell, consisting of 8 photoconverters, can be used to charge one storage battery at the maximum possible air temperatures at surface level. At the same time, the cell is the elementary unit of batteries used for charging any number of storage batteries of any type. The required output voltage is assured by the series-connection of the necessary number of cells, beginning with the required charge voltage.

Table 2 gives the current characteristic of standardized cells for batteries made of silicon photoconverters with an output voltage of 2.8 v for solar radiation of 100 mw/cm^2 and a cell temperature of 30°.

The connection of cells into groups in parallel assures any required battery current.

We also shielded individual cells used to make up a battery,

using plastic or metal boxes. One of these cells is shown in Fig. 3.

The surface utilization factor in such a case is lower than when the individual cells are not shielded, but the convenience, the speed with which batteries can be put together, and the high mechanical strength forces us in certain cases to shield the cells.

The use of metal boxes assures good removal of heat from the photoconverters.

The individual cells on groups that make up the battery are coated with special lacquers when it is necessary to hermetically seal the metal current leads from the harmful effects of the ambient medium and to protect the working surface of the photoconverters from wear.

As we have mentioned, batteries differ greatly in design.

The batteries shown in Figs. 4, 5, 6, 7, and 8 differ in power, size, design, climatic and mechanical resistance, and the shape of the photoconverters used.

Figure 4 shows a battery in an electric table clock and used to recharge the storage battery of the clock. The battery uses round photoconverters connected in series. The battery assures recharging one cadmium-nickel storage battery with currents from 2 to 120 ma for illumination from 100 to 25,000 lux, respectively. The battery case is made of white plastic.

Figure 5 shows a battery for powering an electronic instrument. The battery is in a housing made of a light metal alloy and uses hexagonal photoconverters with radial upper current conductors. Such a battery aggregate makes possible maximum utilization of its area for positioning the photoconverters, but hinders the manufacture of the photoconverters and setting up the battery. The battery is so designed as to be able to be oriented in the vertical plane.

Figure 6 shows a stationary battery used to charge the storage batteries of telemetry equipment. The battery is designed for use in the southern part of the country. The battery case is also made of a light metal alloy and has channels for improving heat transfer with the ambient medium.

The battery design allows it to be periodically reoriented with respect to the sun in horizontal and vertical planes. The battery has devices for changing the type of commutation of the photoconverters in it.

This battery uses seven-element cells with FKD-4 elements. The battery case is 300 mm in diameter. The power of the battery with 100 w/cm^2 incident radiation is about 7 w.

Figure 7 shows a semi-portable battery of folded design with an area of 1 m^2. The battery case is of duralumin and it attached to a stand with extension legs. The design of the battery allows it to be oriented either horizontally or vertically.

The battery is designed for operation under the most adverse climatic conditions, and for transportation by all possible means. The battery consists of round photoconverters. The working surface of the battery is 0.7 m^2; the power with 100 w/cm^2 incident radiation is about 40 w; the battery weighs 10 kg.

Figure 8 shows a portable battery designed for charging the storage batteries of portable small-output radio stations.

The photoconverters are mounted in a closed metal housing which has a strengthening rib which also serves for heat transfer with the ambient air. The battery has special positioning devices and devices for orienting it with respect to the sun. The orientation is controlled by means of a shadow indicator. For control of the operating condition

of the battery and the external electrical circuit it has a special signal device in the form of a pilot bulb which is switched on at the moment of control.

The entire design of the battery assures protection of the photoconverters under any transportation conditions and in any climatic zone of the Soviet Union. The metal parts have rust-inhibiting and wear-resistant coatings. The battery unit includes a connecting cable and a cover for transporting it.

The basic characteristics of the portable battery made of silicon photoconverters are as follows: size 250 × 250 × 20 mm; weight 900 g; output voltage 9 v; output current 450 ma. The voltage and current are given for radiation of 100 mw/cm^2 and a cell temperature of 30°.

Since, for maximum power throughout the daylight part of the day, there must be frequent (at least every 30 minutes) orientation of the battery with respect to the sun's rays, we developed, made, and tested batteries with automatic revolution that would track the sun's rays.

Figure 9 shows such a battery. As the servotransducers we used two groups (6-8 photoconverters) of FKD-2 photoconverters in each plane. The groups of transducers had shields which were so designed that a relay closed the circuit of the executive mechanism when the sun's rays deviated 5-7° from the perpendicular to the plane. The executive mechanisms were powered by storage batteries. The device allowed synchronous tracking both on sunny and on cloudy days, and also automatif rotation of the battery from extreme west to extreme east, in the direction of sunrise. The battery has metallic reflectors.

The use of a servosystem makes it possible to obtain, from batteries with reflectors, 2.5-3 times more energy than from batteries set up in an optimum direction without orientation.

If batteries are used without reflectors, the efficiency of using the servosystem is somewhat lower.

Obviously, with increasing battery power the efficiency of an installation with a servosystem increases. It is expedient in all cases to use reflectors.

We know that the use of mirrors to concentrate the light on the battery makes possible a considerable increase in the specific power of batteries and thus considerably lowers the cost of batteries while retaining their power.

Our investigations made it possible to determine the optimum parameters of the reflecting surfaces (reflectors) and also the real possibilities of using reflectors to increase the specific power of the batteries.

We used individual photoconverters and batteries with surfaces of from 1.5 to 5 dm^2 with metal reflectors.

The load characteristics were recorded under constant solar illumination and constant temperature, and were controlled by means of a control photoconverter. Constant temperature during the measurements was assured by prewarming the battery or the separate photoconverters in the sun until there was equilibrium in the heat transfer between the ambient medium and the test object. The establishment of equilibrium was determined by measuring the emf of the photoconverter or the battery. We considered that equilibrium was established if the emf ceased to drop and remained constant for 15 minutes.

The surface of the batteries was oriented perpendicular to the sun's rays by means of a shadow indicator. The angle of deviation of the surface of the photoconverters from the perpendicular to the sun's rays was established by means of a protractor with an arrow. The

angle-measurement accuracy was $\pm 2^{\circ}$.

Figure 10 shows the principle of operation of the reflectors. The sun's rays, indicent at angle α, are reflected at the same angle onto the surface of the battery. With appropriate selection of the slope of the reflectors with respect to the battery and the magnitude of the reflectors on each elementary plane, the illumination will be the sum of the direct and reflected solar rays. Since the reflected rays strike the surface of the photocells at a large angle, they are partially reflected and will not be used. But the reflected light that is used, as will be shown below, increases considerably (60-140%) the specific power of the battery or the individual photoconverters.

We made seven reflectors of metal foil in the form of the frustrum of a cone whose smaller diameter corresponded to the diameter of the photoconverter in its holder. The length of the generatrix and the slope of the generatrix to the plane perpendicular to the solar battery or the photoconverter are given in Table 3.

In the sunlight we recorded the load characteristics of one photoconverter with reflectors 1, 2, and 3, and without reflectors, for two positions of the photoconverter relative to the sun's rays:

the photoconverter perpendicular to the sun's rays,

the photoconverter turned 25° relative to the perpendicular to the sun's rays.

Figure 11 shows the load characteristics graphically. The dots indicate the points of maximum intensity.

We also recorded the load characteristics of a photoconverter with reflectors 4, 5, 6, and 7 perpendicular to the sun's rays. The load characteristics are shown graphically in Fig. 12. We see that with decreasing slope of the generatrix and a corresponding increase

in its length, the specific power increases somewhat, but the dimensions of the reflectors increase greatly, and the use of reflectors with $\alpha < 30^{\circ}$ is not justified, for all practical purposes. A decrease in the angle of the reflectors requires constant and more precise orientation of the batteries toward the sun.

Thus, for practical use of reflectors, 30° is the optimum slope of α. The magnitude of the reflector should be such that the reflected rays cover the entire photoconverter or battery.

We experimentally determined the increase in specific power of a battery consisting of 40 photoconverters as a function of the area of the metallic reflectors (Fig. 13). The numbers in this figure show the maximum power of a battery without and with reflectors, and the amplification factor K, which is the quotient obtained by dividing the power of a battery with reflectors by the power of a battery without reflectors.

On the basis of obtained data we found the dependence of the battery power on the number (area) of reflectors (Fig. 14). We see that with an increase in the area of the reflectors the battery power increases almost proportionally.

We also studied the possibility of using reflectors to increase the specific power of batteries by means of a battery consisting of 120 series-connected rectangular photoconverters, with an efficiency of 6-8%, joined in series into units of 5 photoconverters each.

The battery surface was oriented perpendicular to the sun's rays by means of a shadow indicator. Metallic mirrors were used as the reflectors. The area of each of the four reflectors was equal to the area of the solar battery.

All measurements were made near Tashkent. We recorded the load

characteristics for a battery with and without reflectors.

The measurement results are shown graphically in Fig. 15.

This figure also shows the points at which the power output of the battery is maximum, and also the power-increase factor when reflectors are used. The power of a solar battery with reflectors is 1.9 times greater than that without reflectors. In all cases there is decreased efficiency of the battery, evidently due to the additional heating of the photocells by the reflected light. The decrease in the order of 8-10%. From Fig. 15 we see that when reflectors are used, the short-circuit current of the battery increases much more than does the power.

Table 4 shows the change in the power-increase factor with a change in battery voltage.

We see that up to a specific voltage, $K > 2$ while with a further increase in the working voltage K begins to rapidly decrease. Our results showed that the use of the simplest reflectors makes it possible to effect a 1.6-2.2 fold increase in the specific power of batteries, and to obtain, from 1 dm^2 of the photoconverters, a power of 1.0-1.6 w with illumination of 100 mw/cm^2.

Recently we have developed a test battery with reflectors. Figure 16 shows such a portable battery with four reflectors. This battery, having a useful photoconverter area of approximately 4.5 dm^2, has an output power of 6.5 w with incident radiation of 100 w/cm^2 and a photoconverter temperature of 30°, which corresponds to a specific power of 1.44 w/dm^2.

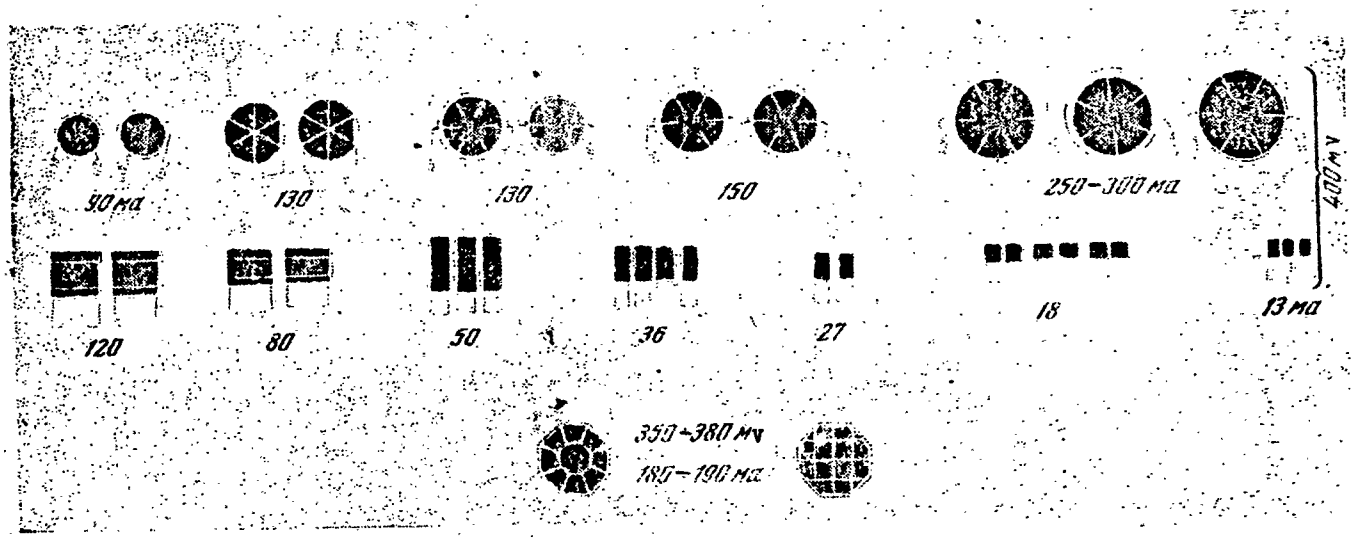

Fig. 1. Types of silicon photoconverters (the lower ones are made of polycrystalline silicon).

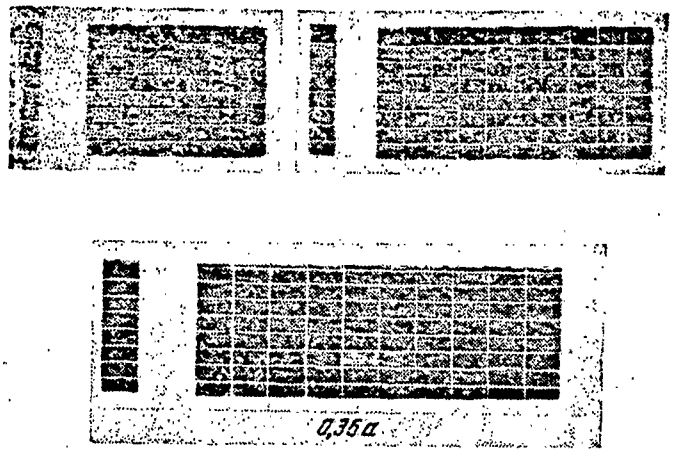

Fig. 2. Types of cells and certain groups of silicon photoconverters.

TABLE 1

Type	Dimensions, mm	Working surface cm^2	Mean efficiency, %	Output current, ma	Output power, mw
FKD -2	10×10	0,85	8	18	7,2
FKD -3	10×15	1,275	8	27	10,8
FKD -4	10×20	1,70	8	36	14,4
FKD -5	10×30	2,40	8	50	20,0

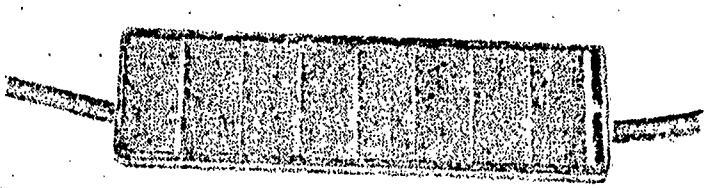

Fig. 3. Shielded cell.

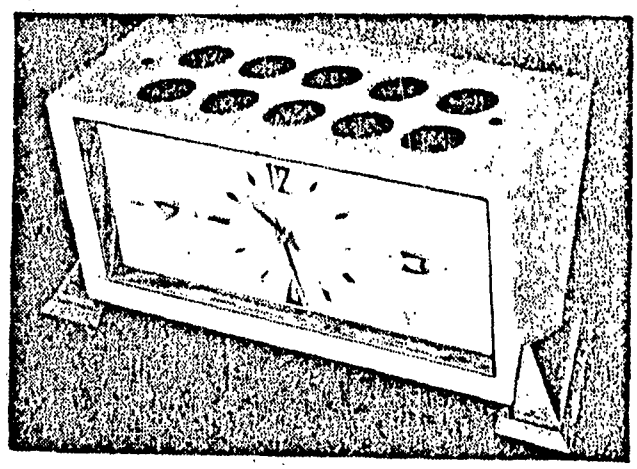

Fig. 4. Battery made of silicon photoconverters in an electric clock.

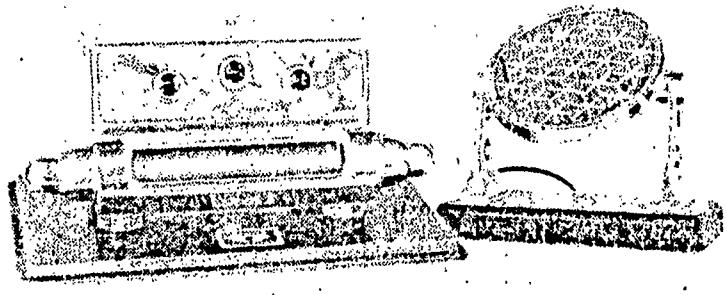

Fig. 5. Silicon-photoconverters battery used to power an electronic device.

TABLE 2

Type of cell	Over-all dimensions, mm	Working surface, cm^2	Output current, ma
8 FKD 2	10×72	6,8	18
8 FKD 3	15×72	10,2	27
8 FKD 4	20×72	13,6	36
8 FKD 5	30×72	19,2	50

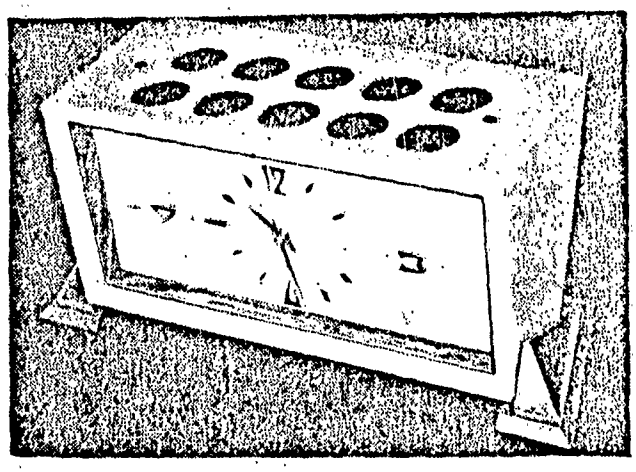

Fig. 4. Battery made of silicon photoconverters in an electric clock.

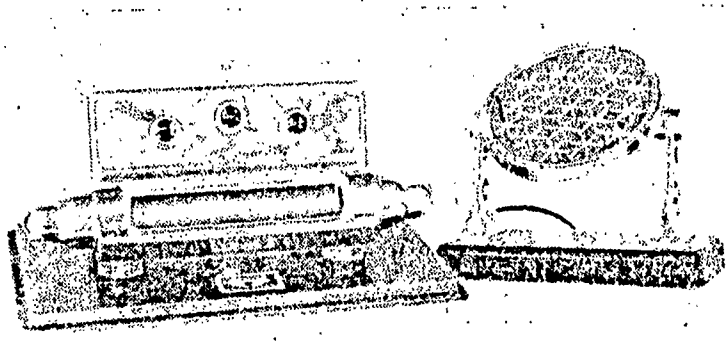

Fig. 5. Silicon-photoconverters battery used to power an electronic device.

TABLE 2

Type of cell	Over-all dimensions, mm	Working surface, cm^2	Output current, ma
8 FKD 2	10×72	6,8	18
8 FKD 3	15×72	10,2	27
8 FKD 4	20×72	13,6	36
8 FKD 5	30×72	19,2	50

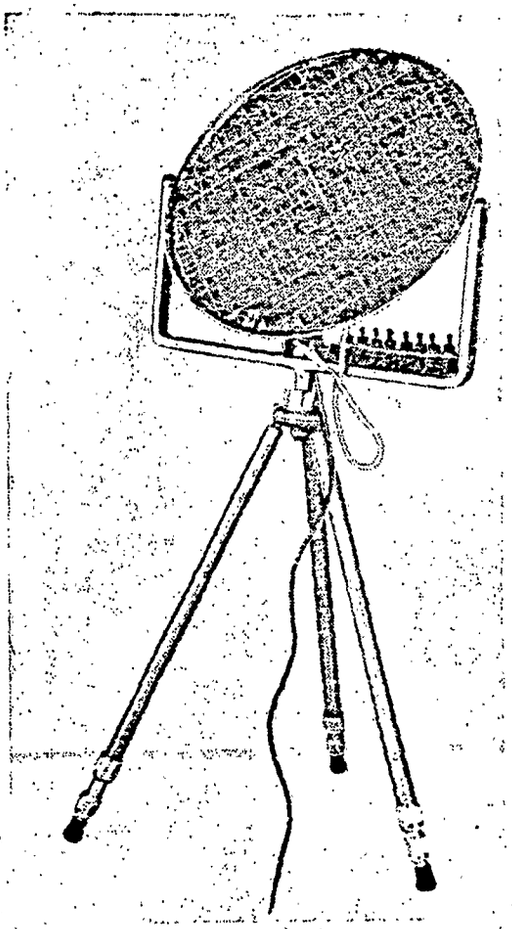

Fig. 6. Stationary battery for charging storage batteries.

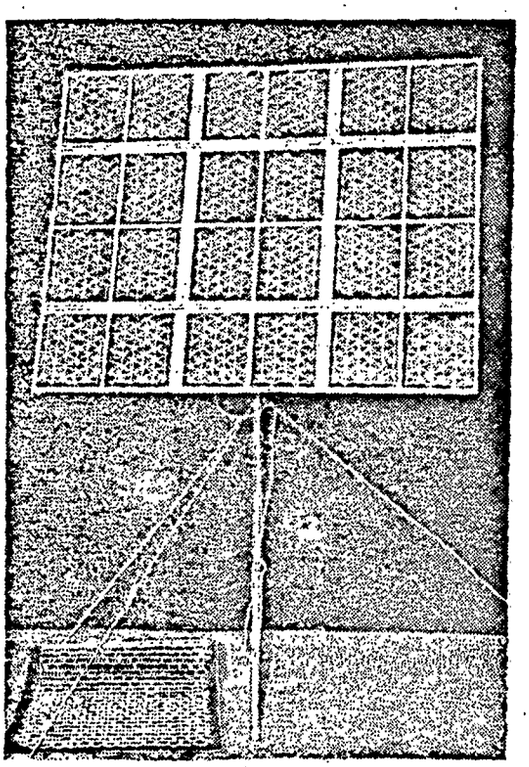

Fig. 7. Semi-portable battery.

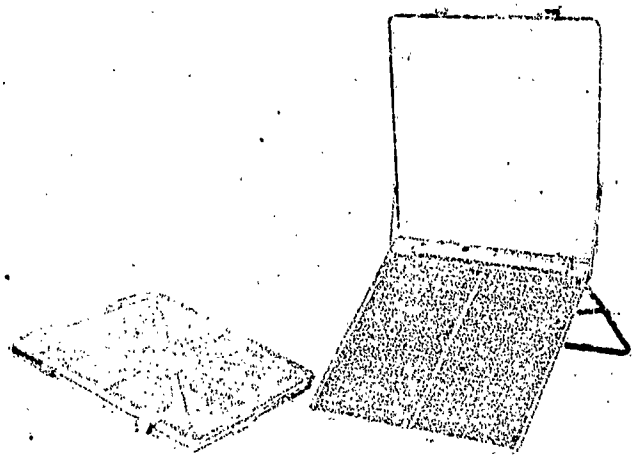

Fig. 8. Portable battery for powering portable radio stations.

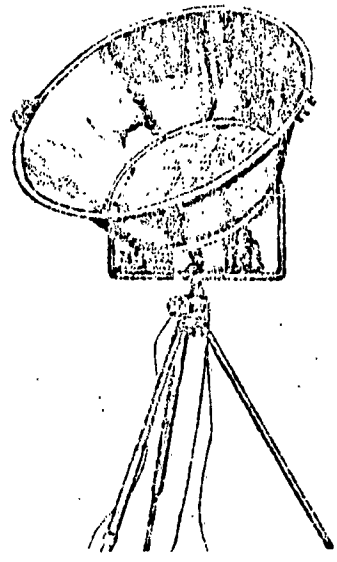

Fig. 9. A battery with automatic revolution.

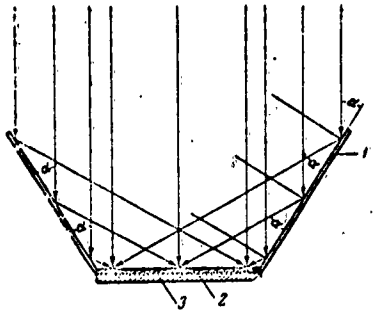

Fig. 10. Principle of reflector operation. 1) reflector, 2) photoconverter; 3) battery housing.

TABLE 3

Reflectors	Slope of generatrix, deg.	Length of generatrix, mm
1	30	34
2	25	34
3	35	34
4	22	60
5	20	72
6	18	84
7	15	110

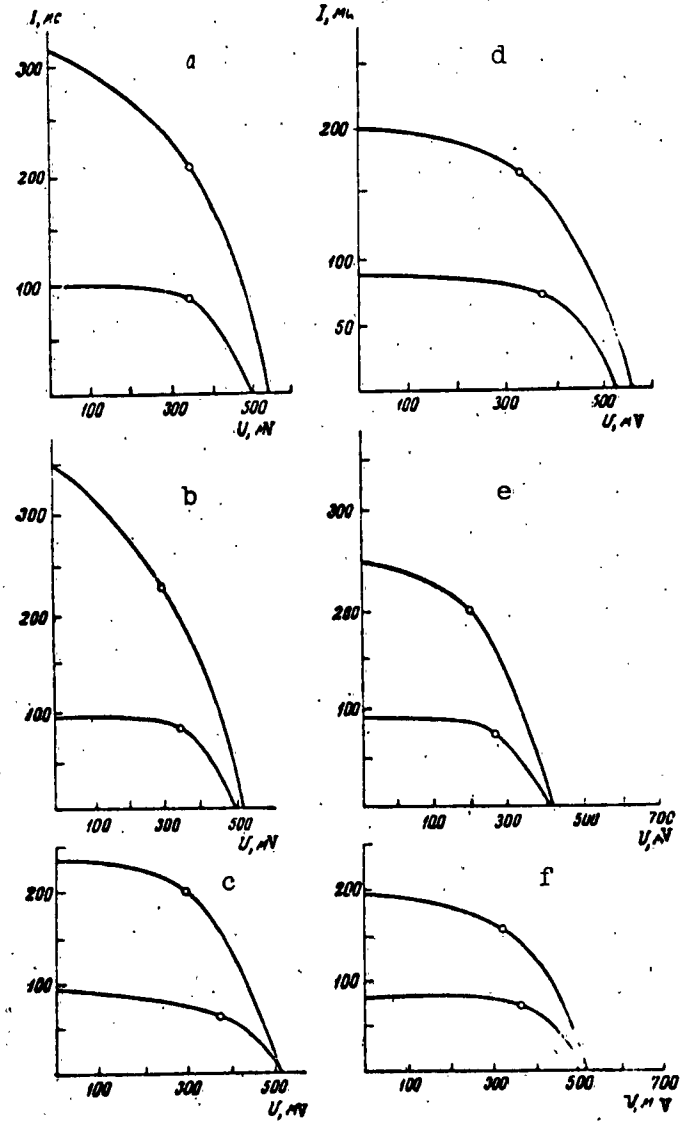

Fig. 11. Load Characteristics of a photoconverter. Upper curves — photoconverter with reflector; lower curves — without reflector. a) $\alpha = 25^{\circ}$; b) 30°; c) 35°; d) 25°; e) 30°; f) 35°; a,b,c) photoconverter perpendicular to sun's rays; d,e,f) not perpendicular.

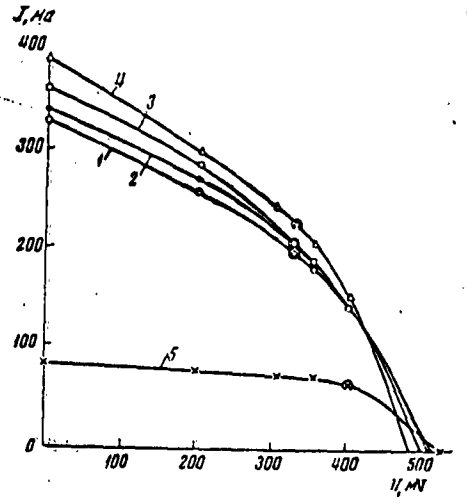

Fig. 12. Load characteristics of a photoconverter without a reflector and with reflectors of various sizes and with various slopes of the generatrix relative to the perpendicular to the battery plane: 1) reflector 4, maximum power 65 mw, K = 2.5; 2) 5, 66.6, 2.56; 3) 6, 66.7, 4; 4) 7, 75, 2.85; 5) no reflector.

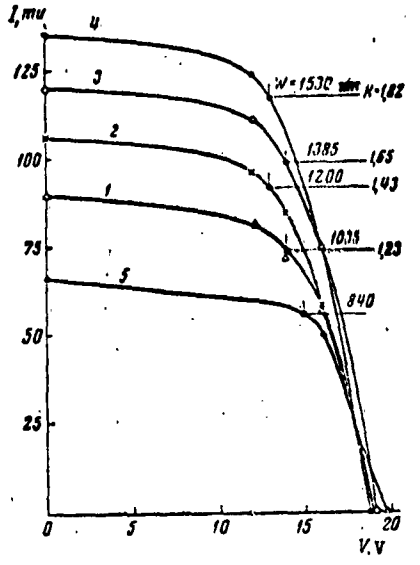

Fig. 13. Loac characteristics of a battery with different numbers of reflectors: 1) with 1 bottom reflector; 2) with a top and bottom reflector; 3) with three reflectors; 4) with four reflectors; 5) without a refeflector.

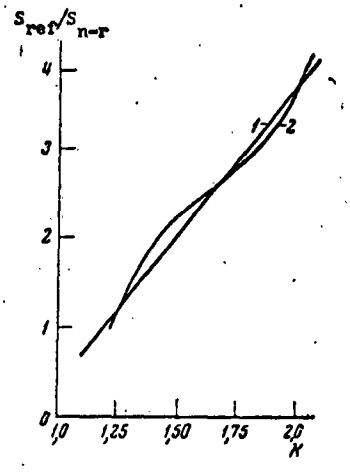

Fig. 14. Battery power vs. area of reflectors with series (1) and parallel (2) connection of the cells of the photoconverters.

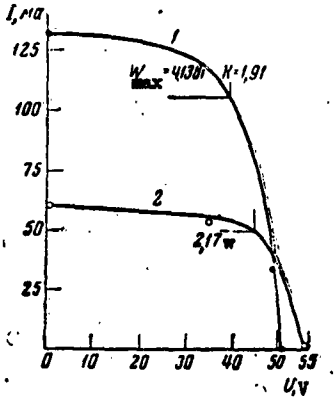

Fig. 15. Load characteristics of an experimental battery with (1) and without (2) metallic reflectors.

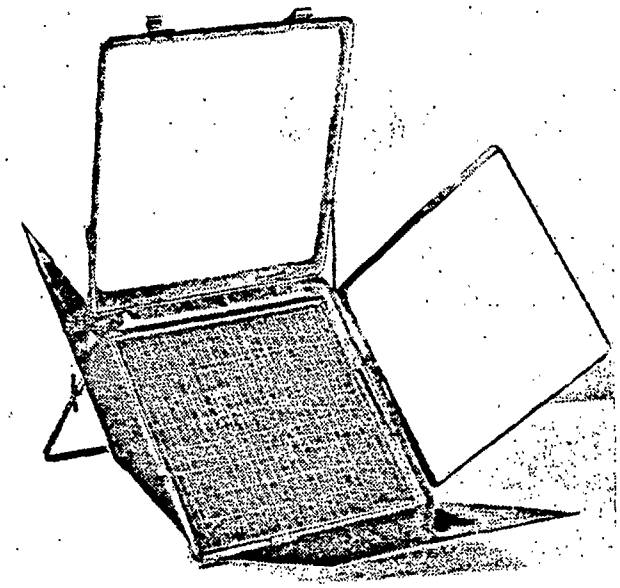

Fig. 16. Portable test battery with four reflectors.

TABLE 4

V, V	Without reflector, W	With reflector, W	K
10,0	0,58	1,30	2,24
20,0	1,14	2,52	2,21
25,0	1,41	3,15	2,24
30,0	1,67	3,66	2,19
35,0	1,90	4,05	2,13
37,5	2,02	4,13	2,05
40,0	2,10	4,11	1,95
42,5	2,17	3,90	1,80
45,0	2,16	3,37	1,56
47,5	2,02	2,50	1,24

INVESTIGATION OF SILICON PHOTOELECTRIC CELLS FOR HIGH CONCENTRATIONS OF SOLAR ENERGY

R. P. Borovikova

Determination of the limiting regimes of the operation of silicon photocells operating with solar-energy concentrators is of great interest. As has been shown [1], silicon photocells manufactured at the Power Engineering Institute of the Academy of Sciences of the USSR had a 20-30 fold increase in output power with 100-150 fold increase in the incident luminous flux. Individual samples produced a 70-fold increase in output power compared with that power generated by the photocell under normal illumination (700-800 w/m^2).

In this work we will investigate silicon photocells with an efficiency from 3 to 10%. The measurement method has been described previously [1].

Thermocouples were soldered to several of the cells to measure the temperature. A depression was formed, by an ultrasound device, in the back of the photocell. The silicon in the depression was etched by a hot 10% KOH solution. After the depression had been washed and dried, the thermocouple bead was placed in it and the depression was filled with drops of In-Ga solder which is a good wetting agent

both for the thermocouple and the silicon.

The cells were first investigated without forced cooling, and then with cooling by running water.

Figure 1 shows the output power of several photocells as a function of the illumination for measurements without cooling. As can be seen from the figure, the output power of the photocells first increases, reaching a maximum at $\Phi = 0.3\text{-}0.5$ w/cm^2, and then decreases. For most of the investigated photocells the output power doubles, compared with that of a photocell at $\Phi = 0.06$ w/cm^2; only for three cells was there a 4- to 5-fold increase. One of the reasons for the slight increase in power and its subsequent drop is probably heating of the photocells. The temperature of the photocells during measurements in natural light fluxes was about 50° (ambient air temperature 35-40°). With an increase in the illumination to 0.4 w/cm^2 the temperature rises to 110°, and it then increases even more — to 200°.

We attempted to investigate the operation of photocells under illumination of 2 w/cm^2. The output power of the photocells dropped to 0.8 mw/cm^2, while the temperature increased so much that the solder melted; the lacquer used to coat the photocell soon burned away, and the contacts came unsoldered (235°).

To eliminate heating of the photocells they were placed in a heat-exchanger which had a transparent bottom made of organic glass. Water at a temperature of 20° was passed through the heat-exchanger. Even with an illumination of 15 w/cm^2 the temperature of the photocells did not exceed 55°.

The results of investigations of photocells cooled in this manner are given in Fig. 2. All cells have an inherent rapid rise in power for illumination up to 4-5 w/cm^2. With a further increase in

illumination, the output power of the photocells remained practically constant, and even dropped in individual cases. An illumination of 4 w/cm^2 corresponded to an approximate 70-fold concentration of the light flux.

Of all the investigated photocells, only one gave a 19-fold increase in power; the others had only a 5-8-fold increase. The variation in power is practically independent of the efficiency of the photocell. From the figure we see that an increase in the illumination of the given photocells above 4 w/cm^2 is impractical, since this would not cause any increase in the specific power. On the other hand, if the photocell operates in a saturation regime, with illumination somewhat higher than 5 w/cm^2, its operation will be stable, and will not depend on random variations in intensity.

On the basis of previous tests, we created a device made from photoelectric batteries with an area of 110 cm^2. The device was cooled with running water. We used a mirror-solar energy concentrator. The device is shown in Fig. 3. The output power of the photobattery, measured under normal illumination of 780 w/m^2, was 0.42 w.

The mirror diameter of 1.4 m was selected so that, taking into account all losses, 500-600 w of energy were incident on the battery with average solar radiation.

To determine the degree of uniformity of the illumination of the photobattery with a mirror, a sheet of asbestos the same size as the battery was placed in the focal plane. The temperature field was recorded by a thermocouple placed at various points of the sheet, in succession (Fig. 4) Nonuniformity of the temperature field results in a considerable decrease in the output power of the photobattery.

The volt-ampere characteristic of the photobattery in the focal

plane of the mirror is shown in Fig. 5. It was recorded for two levels of solar radiation: 570 w/m^2 (crosses) and 719 w/m^2 (dots), which corresponds to illumination of the battery of 4.3 w/cm^2 and 5.4 w/cm^2. The output power of the battery was identical in both cases, and equal to 4.5 w. This indicates that the photobattery operates in a saturation regime in that region where increased illumination has no influence on the value of the output power.

We used a fan motor as the useful load for the photobattery.

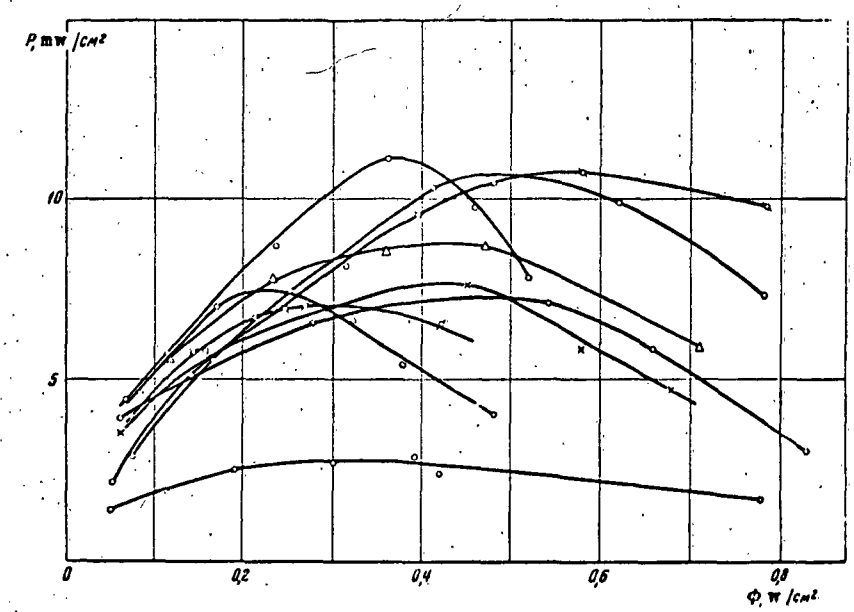

Fig. 1. Output power of various photocells vs. illumination without forced cooling.

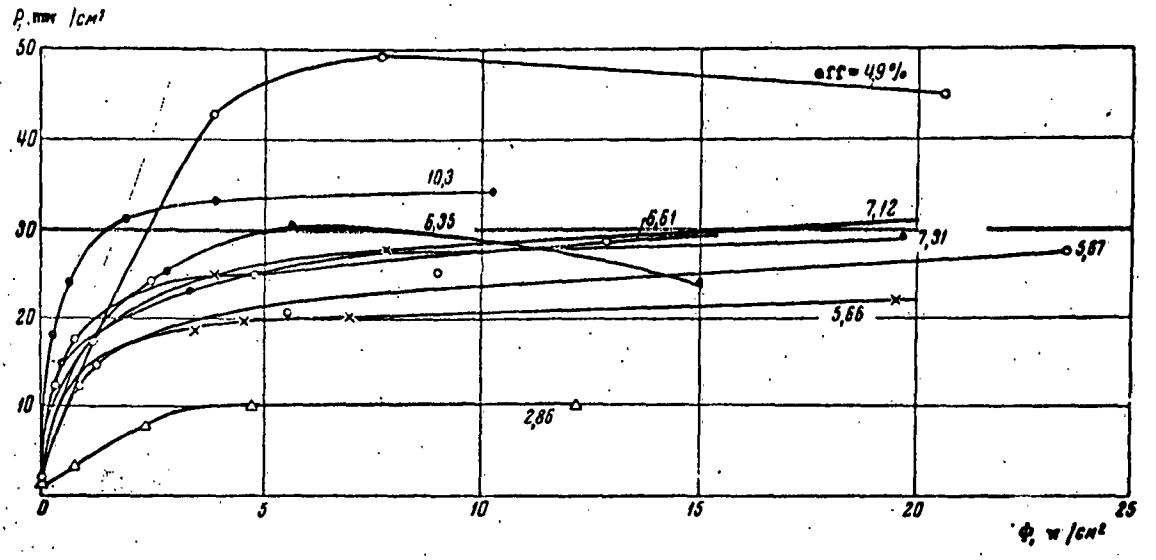

Fig. 2. Output power of photocells vs. illumination when cooled with running water.

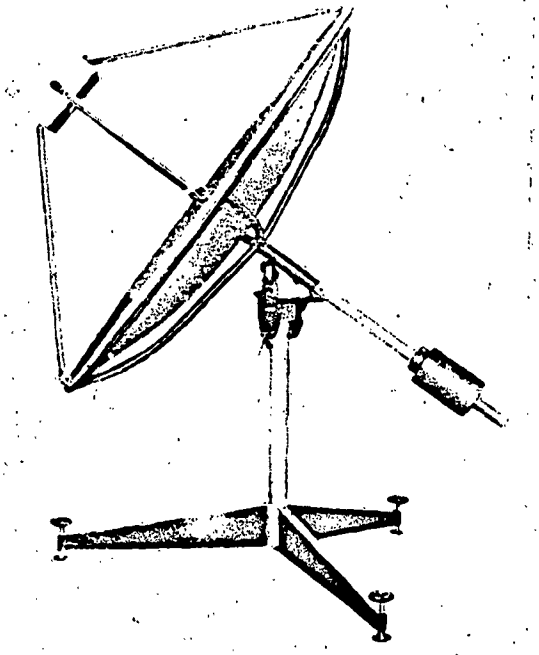

Fig. 3. View of the photobattery with a mirror-concentrator.

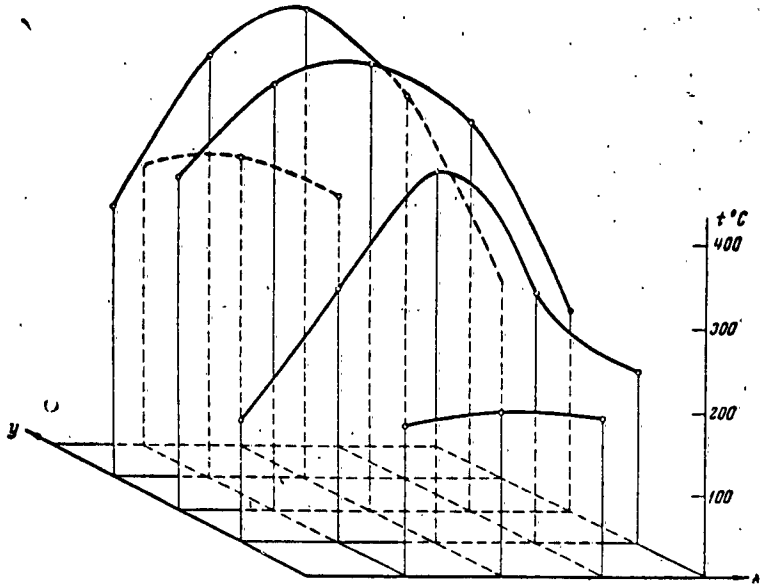

Fig. 4. Temperature field in the focal plane of the mirror.

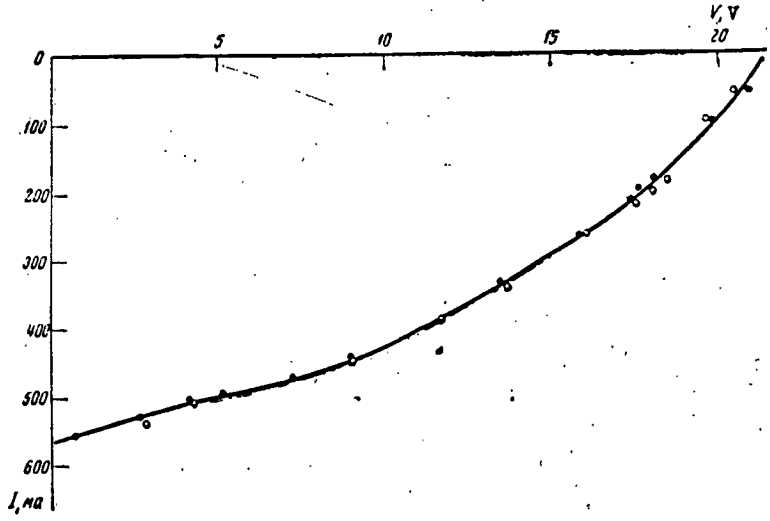

Fig. 5. Volt-ampere characteristic of the photobattery.

REFERENCES

1. V. A. Baum et al. Issledovaniye raboty fotoelementov pri bol'shikh svetovykh potokakh. IFZh, 1960, Vol. III, No. 8.

REFLECTORS FOR SOLAR PHOTOELECTRIC BATTERIES

G. I. Markov

As preliminary experimental, conducted by R. P. Borovikova at the Heliotechnical Laboratory of the Power-Engineering Institute, have shown, the specific power of solar batteries increases considerably with an increase in the concentration of solar radiation. Without touching upon the optimum value of the required concentration factor (which will obviously be refined in the future), let us merely note that even a 4- to 5-fold increase in the concentration will assure a noticeable increase in the specific output of the photobattery, without artificial cooling of its surface being required. An invariant requirement in all cases of the irradiation of solar batteries is their maximum uniform illumination or uniform distribution of the thermal stress in the focal plane of the reflector. This requirement can be fulfilled most simply, particularly for low concentrations, by using beveled parabolic reflectors. Below we give certain general premises and a specific example of the design of such a reflector.

The distribution of stress on a screen with reflection of solar rays from a single plane mirror as a function of the ratio of the size of the mirror and the distance from it to the screen can have varying

form (Fig. 1). Here we assume the following: the mirror has the shape of a flat plate of length a and width B; the rays are incident normal to the mirror; the deviation of the reflected rays from the normal to the mirror, caused by inaccuracies in the preparation of the mirror and by the influence of the angular dimension of the sun, is constant for the entire length of the mirror, and is equal to $\pm\beta$.

Knowing a, β, and L (Fig. 1), it is easy to determine the value of the maximum thermal stress on the screen and L_{cr} at which the stress distribution will correspond to Fig. 1b:

$$L_{cr} = a/2 \tan \beta \qquad (1)$$

Since β is very small, the value of L_{cr} is considerably greater than that of a. Thanks to this, in short-focal-plane installations the stress distribution on the focal plane will correspond to Fig. 1a.

If the rays strike the mirror at some angle $\alpha/2$ (Fig. 2) and if, in addition, the length of the plate $a = 2y$ and $L < L_{cr}$, from Fig. 2 we can easily construct a series of simple equations that express the relation between the values which determine the distribution of the energy reflected by the mirror and α, β, L, and a.

However, the problem can be solved more simply by selecting R', 2y, L, α, and β, and then calculating the values of interest.

As can be seen from Fig. 3, for the zone of uniform energy distribution to be square it is necessary that

$$B_1 = (r_1 + r_1') + 2(r_2 - r_1); \qquad (2)$$

$$B_2 = (r_1 + r_1') + 2(r_2' - r_1'). \qquad (3)$$

Let us calculate a reflector for a photobattery having the form of a square with area $F = 120\ cm^2$. The required concentration K = 4-5.

Let us give the values of β, R', 2y, and α on the basis of the following concepts.

The value of β can be given by starting from the apparent diameter of the sun (32'), ripples or imperfections in the mirror (for a simple mirror made of unpolished glass, the maximum deviation of the reflected ray is $\pm 30'$), and the possible accuracy in aligning the mirrors ($\pm 15'$). Thus the maximum deviation of the reflected ray is $32'/2 + 30' + 15' = 61' \simeq 1^\circ$.

The value of R is given by considering that the photobattery does not shade the mirror and that it is possible to place the required number of mirrors n in a circle of radius R'. In our case, the first condition will be satisfied when $R' > 7.74$, since the radius of the circle described about a square of area $F = 120$ cm^2 will be $r_d = \sqrt{F/2} = 7.74$; the second condition will be satisfied when

$$R' > B_1/2 \tan(360^\circ/2n). \qquad (4)$$

The value of 2y is given by the condition

$$2y > 2r_1 > 2r_d. \qquad (5)$$

The value of α is found from the calculation that the distance L from the center of the bevel to the focal plane is operationally convenient and that it does not exceed one-half the optimum coverage, i.e., 45-50°.

Let us assume that $\beta = 1^\circ$; $R' = 16.0$ cm; $2y = 16.5$ cm; $\alpha = 26^\circ$. Then, from Fig. 2,

$$R = R' + y\cos\alpha/2 = 24{,}04;$$
$$R'' = R + y\cos\alpha/2 = 32{,}08;$$
$$h = 2y\sin\alpha/2 = 3{,}71;$$

$$L = R\tan(90^\circ - \alpha) = 49{,}29;$$

$$L' = L - \frac{h}{2} = 47{,}43;$$

$$L'' = L' + h = L + \frac{h}{2} = 51{,}14;$$

$r_1 = L''\tan(\alpha - 1^\circ) = 7{,}85$, i.e. $16{,}5 > 15{,}7 > 15{,}48$ according to Formula (5);

$$r_2 = L''\tan\alpha = 8{,}94;$$

$$r_3 = L''\tan(\alpha + 1^\circ) = 10{,}6;$$

$r_1' = R'' - L'\tan(\alpha + 1^\circ) = 7{,}81$, i.e. $16{,}5 > 15{,}62 > 15{,}48$;

$$r_2' = R'' - L'\tan\alpha = 8{,}95;$$

$$r_3' = R'' - L'\tan(\alpha - 1^\circ) = 9{,}96.$$

The maximum thermal stress at the focal point of a single mirror can be determined from the following concepts.

Let the stress of direct solar radiation be S, in cal/cm^{2}min. Then, the stress of the direct solar radiation on a flat mirror, the normal to which forms the angle $\alpha/2$ with the direction of the solar rays, will be

$$S_1 = S \cos \alpha/2 = 0.974S.$$

If the coefficient of reflection of the mirror $R_3 = 0.8$, the stress of the direct solar radiation after reflection onto the focal plane, the normal to which forms the angle α with the direction of the reflected rays, will be

$$S_2 = E_{max_1} = S_1\ 0.8 \cos \alpha = 0.700S.$$

The required number of facets is determined from the formula

$$n = K/E_{max_1}. \qquad (6)$$

When n = 6, the maximum thermal stress on the focal plane from 6 facets will be

$$E_{max} = nE_{max_1} = 4.2S,$$

which satisfies our requirements.

The width of the facets, according to Formulas (2) and (3), will be

$$B_1 = 17.84;\ B_2 = 17.94,$$

while

$$B_1/2 \tan (360^\circ/2n) = 15.45 < 16.0,$$

which satisfies the second requirement on the ratio R' expressed by Formula (4).

Figure 4 shows the general form of a reflector which in our case might better be called a beveled cone; Fig. 5 shows the light spot and the stress distribution on the focal plane of this reflector.

From an examination of Fig. 5 we can easily determine the other values of interest in our case:

$$r_4 = \frac{r_{1\,\min}}{\cos 15^\circ} = 8{,}09;$$
$$r_5 = \sqrt{2r_{1\,\max}^2} = 11{,}10;$$
$$r_6 = \sqrt{2r_{2\,\max}^2} = 12{,}66;$$
$$r_7 = \sqrt{2r_{3\max}^2} = 14{,}44;$$
$$r_8 = r_6 + (r_3 - r_2) = 13{,}78;$$
$$r_9 = \frac{r_7 \sin 45^\circ}{\sin 60^\circ} = 11{,}79;$$
$$r_{10} = r_8 \cos 15^\circ = 13{,}31.$$

The area of the square (photobattery) inscribed in a circle of radius $r_{1\,\min} = 7.81$.

$$F_1 = 2r_1^2 = 122.0\ \text{cm}^2;\ \text{given:}\ \ F_1 = 120\ \text{cm}^2.$$

It is clear that with some other form for the photobattery, its area could be increased considerably. For a photobattery in the form of a rectilinear hexagon, its area

$$F_2 = {}^3/_2 r_1 \sqrt{3} = 158{,}8\ см^2.$$

For a photobattery in the form of a rectilinear octagon, its area

$$F_3 = 8r_1^2 \tan\frac{360^\circ}{16} = 172{,}6\ см^2.$$

Finally, for a round photobattery, its area might reach

$$F_4 = \pi r_1^2 = 191{,}5\ см^2.$$

The results of these calculations can be verified as follows. Obviously, the amount of energy incident on the focal plane V should equal the amount of energy reflected from all six mirrors Q_{ref}.

With reasonable accuracy we can write

$$V = \frac{\pi}{3}(R_1^2 + R_2^2 + R_1 R_2) H,$$

where

$$R_1 = \frac{1}{2}(r_1 + r_4) = 7{,}95;$$

$$R_2 = \frac{1}{2}(r_5 + r_8) = 12{,}78;$$

$$H = 4{,}2S.$$

Then V = 1442S.

The value of Q_{ref} is determined by the formula

$$Q_{ref} = S6R_3 \frac{B_1 + B_2}{2} \cdot (R'' - R') = 1429\,S.$$

Consequently, we get $V \simeq Q_{ref}$.

By increasing the number of facets n and positioning them in concentric rings, we can considerably increase the obtained concentration, still retaining the uniform distribution of stress in the greater part of the focal spot.

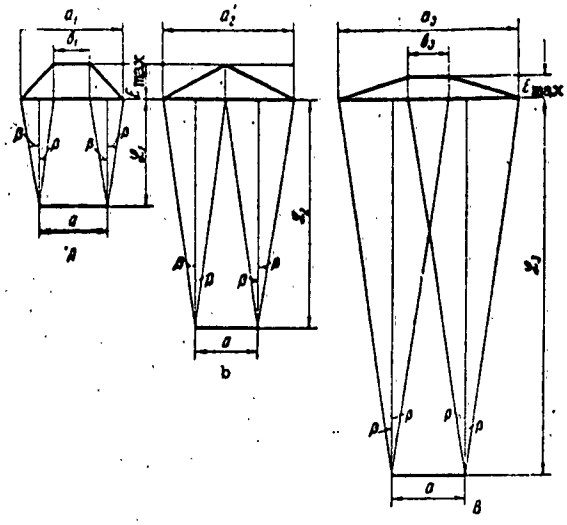

Fig. 1. Distribution of stresses on a screen with reflection of rays from a mirror plate of infinitely small width (the rays are incident normal to the plate).

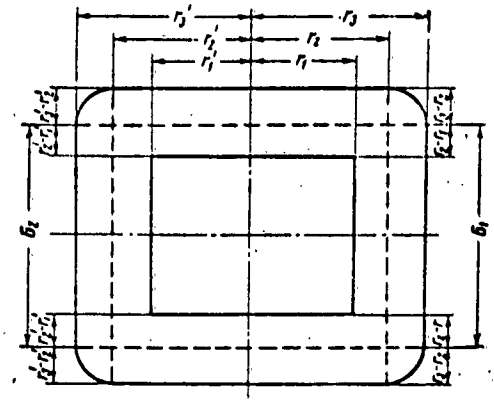

Fig. 3. Light spot on the screen with reflection of the rays from a single rectangular mirror.

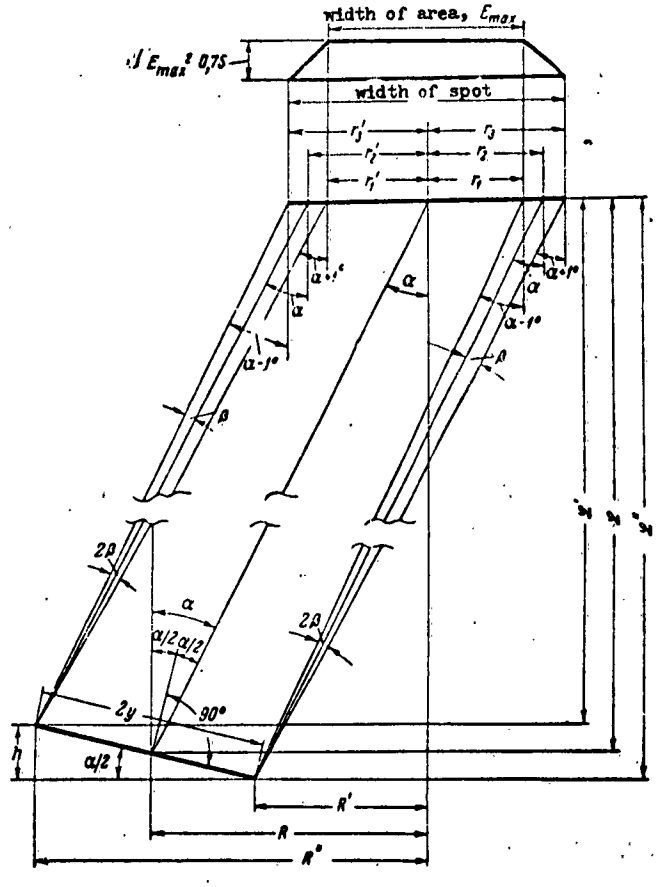

Fig. 2.. Geometric diagram for designing a beveled reflector.

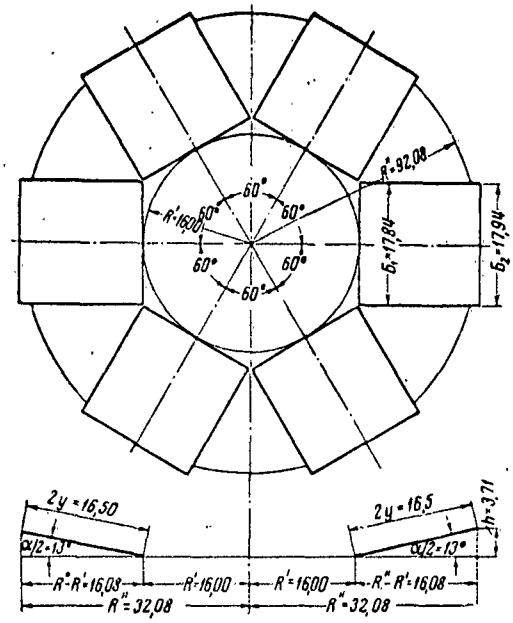

Fig. 4. Plan and cross section of a beveled reflector with uniform distribution of thermal stress (K = 4.2S) for most of the light spot.

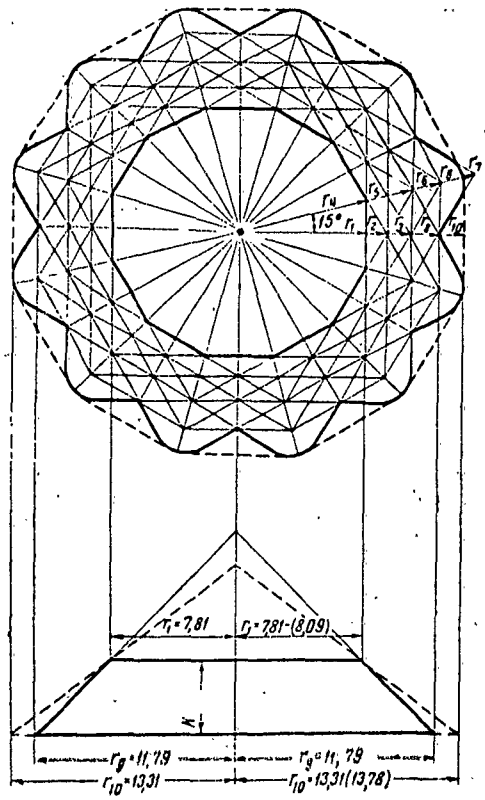

Fig. 5. Light spot and stress distribution on the focal plane of a beveled reflector when K = 4.2S.

DISTRIBUTION LIST

DEPARTMENT OF DEFENSE	Nr. Copies
HEADQUARTERS USAF	
AFCIN-3D2	1
ARL (ARB)	1
OTHER AGENCIES	
CIA	1
NSA	6
DIA	9
AID	2
OTS	2
AEC	2
PWS	1
NASA	1
ARMY	3
NAVY	3
NAFEC	1
RAND	1
PGE	12

MAJOR AIR COMMANDS		Nr. Copies
AFSC		
SCFDD		1
ASTIA		25
TDBTL		5
TDBDP		5
AEDC	(AEY)	1
APGC	(PGF)	1
SSD	(SSF)	2
ESD	(ESY)	1
RADC	(RAY)	1
AFMTC	(MTW)	1
ASD	(ASYIM)	1